GENERALIZED SPECTRAL MODEL FOR 1–100 keV X-RAY EMISSION FROM CYGNUS X-3 BASED ON *EXOSAT* DATA

M. R. Rajeev, V. R. Chitnis, A. R. Rao, and K. P. Singh
Tata Institute of Fundamental Research, Homi Bhabha Road, Bombay 400 005, India
Received 1992 December 28; accepted 1993 September 27

ABSTRACT

The X-ray spectrum of the highly variable X-ray source, Cyg X-3, has so far defied a consistent explanation based on simple emission models. We have extracted two of the best data sets from the *EXOSAT* archives and performed a detailed spectral analysis for its "high" and "low" states. The analysis of the less frequently occurring "low" state is presented for the first time for the *EXOSAT* data. Combining data from the medium-energy argon and xenon detectors and the gas scintillation proportional counter, with a better energy resolution, and carrying out a simultaneous fit, we find that the X-ray continuum in both the "high" and "low" state can be explained as a sum of a blackbody emission and emission from a Comptonized plasma cloud with a common absorption. The Comptonization model is sufficient as well as preferable to many other models, in explaining the observed X-ray emission up to 100 keV. In addition, we find an emission-line feature due to ionized iron (Fe xx–Fe xxvi) and absorption features due to cold iron (Fe i) as well as highly ionized iron (Fe xxv–Fe xxvi). The presence of absorption due to Fe i has been shown for the first time here. This is the simplest and the most generalized spectral model for the 1–100 keV X-ray emission from Cyg X-3, to date.

We find that the blackbody temperature derived in the "high" state (1.47 keV) is much lower than that derived for the "low" state (2.40 keV) and is associated with an increase in the blackbody radius in the "high" state. The ratio of blackbody flux to the total flux is ~ 0.61 in the "high" state and ~ 0.44 in the "low" state. The Fe line energy is significantly higher in the "high" state (~ 6.95 keV) compared to the "low" state (~ 6.56 keV). The Comptonization parameter changes from 2 to ~ 15 in going from the "high" to the "low" state implying a highly saturated Comptonization in the "low" state. The Comptonized region has high electron temperature and low opacity in the "high" state and vice versa in the "low" state. The orbital light curve is mostly explained by variations in the intensities of the continuum components. We discuss the likely origin of different emission regions, continuum and line, and interpret them in terms of an accretion disk corona.

Subject headings: binaries: close — stars: individual (Cygnus X-3) — X-rays: stars

1. INTRODUCTION

The X-ray binary, Cyg X-3, is among the brightest X-ray sources in the sky with a highly variable luminosity ~ 2–10×10^{37} ergs s^{-1} in the 2–10 keV band (for an assumed distance of 8.5 kpc). It is situated in the Galactic plane and has been observed in almost all the regions of the electromagnetic spectrum. The X-ray emission from Cyg X-3 has a stable, smooth but asymmetric 4.79 hr modulation (amplitude $\approx 50\%$ in the 2–10 keV region), which is ascribed to its binary motion. The source exhibits a "high" state and a "low" state with no apparent regularity, but the "high" state occurring more often than the "low" state (see Bonnet-Bidaud & Chardin 1988 for a review).

Despite a number of observations of Cyg X-3 over the past two decades, a general characterization of its X-ray spectrum has remained elusive. Many different models have been proposed for its continuum, and there has been a universal lack of statistically acceptable fits to its data. A soft component below 2 keV, invariably modeled as thermal bremsstrahlung of temperature $kT \sim 0.3$ keV and reported to be seen more clearly when Cyg X-3 is in its "low" state, is most probably external to the source (White & Holt 1982) and could be from the hot OB stars of the nearby association Cygnus OB2 (Harnden et al. 1979). Above 2 keV its continuum has been modeled as a blackbody with a temperature of about 1 keV (Sanford, Mason, & Ives 1975; Serlemitsos et al. 1975; White & Holt

1982; Kitamoto et al. 1987) or thermal bremsstrahlung with $kT \simeq 3$ keV (Becker et al. 1978; Blisset, Mason, & Culhane 1981) or a power law (Becker et al. 1978; Willingale, King, & Pounds 1985). The use of a blackbody in the "high"-state spectrum was invariably accompanied by the presence of a second component modeled as a power law (energy index, $\alpha \sim 1$–2) (White & Holt 1982; Kitamoto et al. 1987), whereas for the "low" state a single-component power law ($\alpha \sim 0.1$) was found to be adequate (White & Holt 1982). A significant absorption with the equivalent H i column density ranging from 3 to 12×10^{22} cm^{-2} has been reported based on different models for the continuum. There is, however, no evidence to suggest that the 4.8 hr variation is related to absorption (Blisset et al. 1981; White & Holt 1982; Kitamoto et al. 1987), and it has not been possible to isolate the component responsible for these variations. In the energy region of 20–100 keV a simple power law ($\alpha \sim 2.2$) has been found sufficient to describe the data (Hermsen et al. 1987; Rao, Agrawal, & Manchanda 1991).

Intense line emission in the energy range of 6–7 keV has been detected in all the observations. The line centroid has been quoted between 6.3 keV and 6.8 keV with a tendency toward the lower energy during the maxima in the light curve (Becker et al. 1978; Blisset et al. 1981). This trend, however, is not confirmed by higher resolution *Tenma* observations (Kitamoto et al. 1987). The line widths reported from different experiments are not mutually consistent, with the observations

using proportional counters showing larger widths (FWHM) of ~1 keV (Becker et al. 1978; Blisset et al. 1981; White & Holt 1982) compared to the observations with gas scintillation proportional counters which show a smaller width of ~0.5 keV (van der Klis et al. 1985; Kitamoto et al. 1987). The interpretation by White & Holt (1982) of the larger width as consisting of two components, one at 6.7 keV and the other at 6.4 keV, is also not substantiated by the *Tenma* results (Kitamoto et al. 1987). A similar controversy surrounds the variation of line flux correlated with the continuum flux. Such a correlation has been reported by van der Klis et al. (1985) but found to be nonexistent by Kitamoto et al. (1987). The source of line emission is, therefore, uncertain. An absorption edge at ≈ 9.2 keV has also been reported (Kitamoto et al. 1987).

The lack of a consistent model for the continuum and line emission of Cyg X-3 and the proper identification of the variable parameters have hampered the understanding and modeling of the emission regions in the source. It is with the objective of obtaining a general spectral model for Cyg X-3 that we have analyzed the broad-band (1–50 keV) X-ray spectral data obtained using the detectors aboard the *EXOSAT Observatory*. In a novel attempt, data from the three principal detectors, viz., the Gas Scintillation Proportional Counter (GSPC) and the argon- and xenon-filled proportional counters in the medium-energy detector have been *analyzed jointly for a simultaneous fit to models*, thus exploiting the higher bandwidth of the ordinary proportional counters for a proper definition of the continuum along with the higher resolution of the GSPC for the line studies. Two observations corresponding to a "high" state and a "low" state of Cyg X-3 have been analyzed in search for a universal explanation of the spectral shape as a function of the binary phase and the intensity states. A detailed spectral analysis of a "low"-state observation with *EXOSAT* is being presented here for the first time.

The paper is organized as follows. In § 2 we explain the data selection and the details of the observations. In § 3 we describe the various spectral emission models that are likely to be present in the Cyg X-3 spectra. In § 4 we describe the spectral analysis and results obtained which includes the details of the method followed by us in arriving at the generalized spectral model (§§ 4.1, 4.2, and 4.3), an overview of the major results in the two intensity "states" of the source (§ 4.5). The results are discussed in § 5 followed by a summary in § 6.

2. THE *EXOSAT* DATA

The *EXOSAT* database contains 22 observations on Cyg X-3 of which only about four observations were made when the source was in the "low" state. Seventeen observations have been analyzed to obtain the binary ephemeris (van der Klis & Bonnet-Bidaud 1989) and five observations have been analyzed to look for short-duration (few hundred seconds) flux variability (van der Klis & Jansen 1985). The data from the medium-energy (ME) detector obtained on 1983 July 3–5 (Willingale et al. 1985) and the GSPC data obtained on 1983 July 3–5 and 1983 October 26 (van der Klis et al. 1985) are the only spectral results presented so far from the *EXOSAT* database on Cyg X-3, and these data pertain to "high" state only. In this paper, in order to model the spectrum better, we have chosen two observation periods corresponding to the different states of Cyg X-3. The "high"-state data are from the observation carried out on 1983 October 26 and has an ME count rate that is higher than the 1983 July 3–5 observation by a factor of ~1.3. For the "low" state, we have chosen the observation

carried out on 1984 May 21, which is the only "low"-state observation in the *EXOSAT* data base *with sufficient binary coverage and sufficient channel resolution* in the GSPC. These two observations will be referred by the year and day number of observations, 1983/299 and 1984/142, respectively.

The data were obtained from the *EXOSAT* archives. Analysis was performed starting with data from FOTs (First Observation Tapes) and using the X-ray Analysis and Data Utilization (XANADU) package. The spectral analysis was carried out using the XSPEC software (Shafer et al. 1991). The ME data were obtained from argon-filled (Ar) detectors as well as from Xenon-filled (Xe) detectors. The GSPC, although having a small area (≈ 150 cm^2), has an energy resolution that is a factor of 2 better than the Ar detectors (Peacock et al. 1981). The GSPC was operating at gain 2 (Peacock et al. 1981) covering an energy range of 2–16 keV in 256 pulse height (PH) channels, for both the observations. The Ar and Xe detectors are more sensitive as they have an area of ~1600 cm^2. The energy range in which the Ar detectors are sensitive is 1–20 keV, whereas the Xe detectors are sensitive between 5 and 50 keV (Turner et al. 1981).

The ME detectors normally operate as two arrays, each consisting of four detectors and collectively known as the half 1 array and the half 2 array, respectively. The ME observations on 1983/299 were carried out exclusively by the half 1 array. The half 2 array was offset from the source and monitored the background simultaneously. The ME data of 1984/142 were from both the half 1 and half 2 arrays as they were co-aligned. The background rates for a given half-array was derived while the same array was slewing toward and away from the source. In the 1983 observations the background rates were stable at the beginning and the end of the observations. In the 1984 observations, however, there is an indication of a slow change in the background, which is negligible for the Ar detectors (~2%) and ~7% for the Xe detectors. The correctness of the background subtraction was verified by examining the data at higher energies where the source contribution is negligible (cf. Singh, Rao, & Vahia 1991). The 1983 ME data were acquired in 128 PH channels each for the Ar and Xe detectors. However, the 1984 ME data were acquired in 32 PH channels, thereby restricting the data from the Xe detectors to 31 keV. Data from the Xe detectors extended up to 50 keV.

The GSPC data, obtained contemporaneously with the ME data, also acquired background data during the slew maneuver. The standard long-duration background observation of GSPC was, however, used after scaling for the current gain (determined from the background lines—see below).

The "high"-state observations were carried out for 2.2 binary cycles of Cyg X-3, starting on 1983 October 26 01:04:03 UT (corresponding to the Cyg X-3 binary phase of 0.10), while the "low"-state data cover about 1.2 binary cycles starting on 1984 May 21 14:35:00 UT (binary phase 0.55). The binary phases were derived from the quadratic ephemeris given in van der Klis & Bonnet-Bidaud (1989). The detected count rates after correcting for vignetting, dead time, etc. are given in Table 1. For proper comparison, the count rates are presented for one complete binary cycle in each of the observations. The background-subtracted light curves of Cyg X-3 obtained from the Ar half 1 detectors in the 3–10 keV range for 1983/299 and 1984/142 are shown in Figure 1. Similar light curves from Xe detectors in the 10–30 keV range for 1983/299 and 1984/142 observations are shown in Figure 2. The light curves displayed, for the two observations, have a time resolution of 100 s. The

TABLE 1

AVARAGE COUNT RATES FOR ONE BINARY CYCLE

Detector	Energy Range (keV)	Count Rate (counts cm^{-2} s^{-1})
1983 Oct 26 (1983/299)		
GSPC	3.0–10.0	0.3161 ± 0.0006
ME argon (half 1)	3.0–20.0	0.4698 ± 0.0003
ME xenon (half 1)	5.0–50.0	0.0521 ± 0.0006
1984 May 21 (1984/142)		
GSPC	3.0–10.0	0.1260 ± 0.0004
ME argon (half 1)	3.0–20.0	0.1751 ± 0.0006
ME argon (half 2)	3.0–20.0	0.1672 ± 0.0006
ME xenon (half 1)	5.0–30.0	0.0646 ± 0.0008
ME xenon (half 2)	5.0–30.0	0.0629 ± 0.0008

results are presented as a function of binary phase. As noted by previous observers (Elsner et al. 1980; van der Klis & Bonnet-Bidaud 1989) the similarity of the light curves near the zero phase, the large fluctuations, and the cycle-to-cycle variations in the 0.2–0.6 binary phase region are evident in Figures 1 and 2.

2.1. Mutual Detector Calibration of ME and GSPC

We performed a careful check on the energy scale and mutual area calibration of the three detectors (Ar, Xe, and GSPC). The Ar detector is the most used and best understood of all the three nonimaging detectors in the *EXOSAT Observatory*, and we have suitably adjusted the energy gain and areas

of the Xe and GSPC detectors with respect to the Ar detector. These adjustments were minor but significant.

From an observation of the Crab Nebula, the Ar and Xe detectors have been intercalibrated (Smith & Parmar 1985). To allow for any systematic differences in the effective areas of the Ar and Xe detectors, we attempted a combined fit to the Ar and the Xe detector data with two continuum components and a Gaussian line near 6.6 keV with absorption edges (see below). Spectral data were obtained with integration time corresponding to the binary phase of 0.2, and the resulting residuals from the Ar and Xe detectors were carefully examined for each of the spectral files. It was found that a correction factor corresponding to a 3% increase in the area of the Xe detector half 1 array had to be applied, for the 1983 and the 1984 observations. For the Xe detector half-2 array (only 1984 observations), no corrections were required.

The gain of the GSPC detector can be accurately determined using two background line features at 10.5 and 12.7 keV caused by fluorescence in the lead collimator and the radioactive decay of residual plutonium in the beryllium window, respectively (White & Peacock 1988). The energy (E) to channel (N) relationship (White 1985) for the GSPC is given by the relation

$$E = (N - 1.5)G + 0.140 ,$$

where G is the gain parameter. To investigate any possible gain variations during the period of observations, we examined the on-source data, without background subtraction, for the location of the background lines. We then modeled the data in the 9–14 keV energy region as a power law and two Gaussian lines. The energies and the widths of the Gaussian lines were
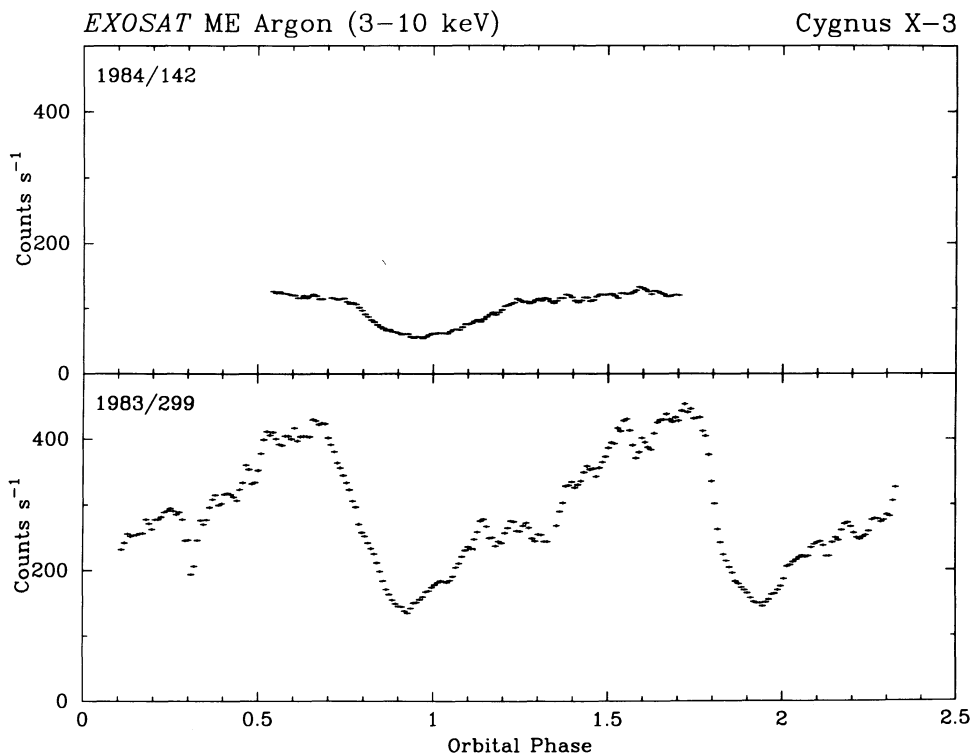

FIG. 1.—Background-subtracted light curve of Cyg X-3 obtained from the *EXOSAT* ME argon half 1 detectors in the 3–10 keV range is shown with a time resolution of 100 s, for the 1983 October 26 (1983/299) and the 1984 May 21 (1984/142) observations. The binary orbital phase is calculated using the quadratic ephemeris given by van der Klis & Bonnet-Bidaud (1989).
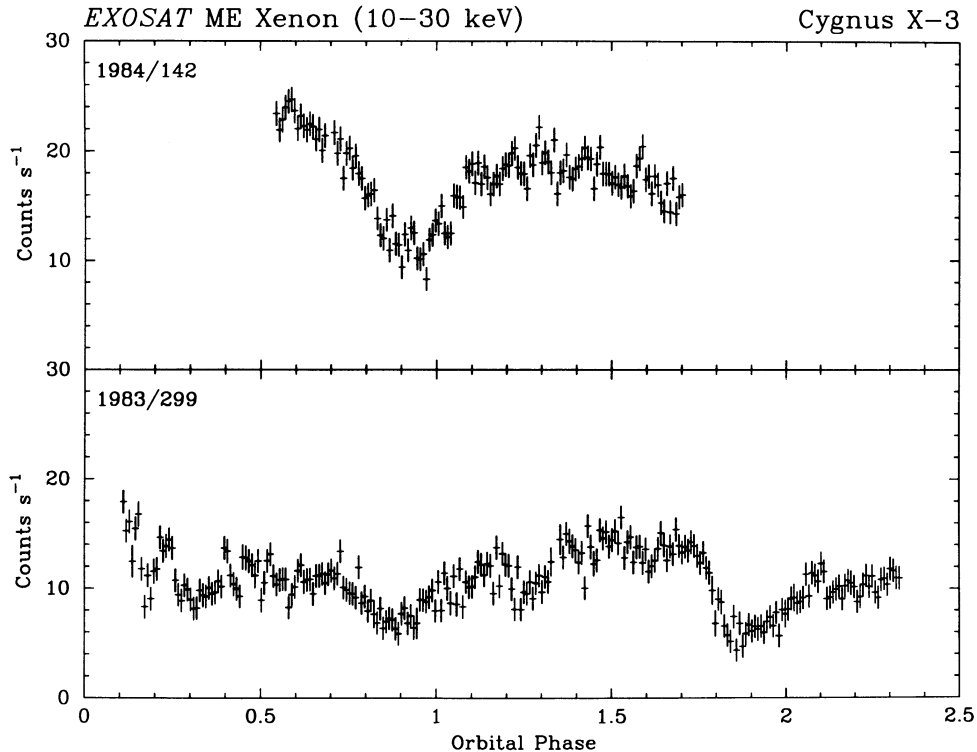
FIG. 2.—Same as Fig. 1, but the data are from the *EXOSAT* ME xenon detectors, in the energy range of 10–30 keV

frozen, and the model was convolved through various detector response functions with different values of G and fitted to the data. In Figure 3 the values of χ^2_{min} obtained from the above fitting procedure, using response functions derived for various values of G are shown for the 1984 data. The analysis was done for spectra taken at four different but consecutive integration times (numbered sequentially in Fig. 3) of duration ~ 5000 s. The minimum value of χ^2_{min} (about 70 for 64 degrees of freedom—dof) was found to correspond to the same value of G for the four data sets, indicating that the gain was stable during the period of observation. We could determine the value of G correct to 0.3% by this method. The source contribution was much higher in the 1983 observations, and hence the value of G could be determined only to an accuracy of about 0.6%. In addition to this, during the 1983 observations, the gain varied by about 1.8% from the beginning to the end of observations.

From an analysis of the Ar and the GSPC spectra of the supernova remnant Cas A (Singh 1992), it was found that the relative energy scales of Ar and GSPC can differ by $\sim 1\%$ and the relative effective areas by $\sim 3\%$. It was also found that these variations differ slightly from observation to observation. We have obtained the relative gain and effective areas of these two detectors by attempting a combined fit to the Cyg X-3 data, taken at a binary phase interval of 0.2. We found that for the 1984 data, where the GSPC gain was stable correct to 0.3%, the GSPC and Ar gains and effective areas agreed with each other. For the 1983 observations, corrections correspond-ing to 1.5% increase in the GSPC gain and a 2% increase in its effective area were required. The Xe and GSPC data were noisier than the Ar data, and a 1% systematic error was included for these data. As mentioned earlier, the ME back-ground showed slight variation during the 1984 observations, and a systematic error of 1% was needed for this Ar data.

The background subtraction at those energies at which the background count rates are dominant was examined critically. The GSPC data were restricted to be between 2.7 and 10.0 keV due to interference of the background lines at higher energies and improper background subtraction at lower energies. For the Ar detectors we went down to ~ 1 keV, in the 1983 data, as this was the lower limit from the 1984 data. The upper limit was set to 20 keV as above this value the efficiency of Ar detector is much lower than that of the Xe detector. For the Xe detector we have covered the range from 5 keV right up to 50 keV in the 1983 data as the source contribution is almost nil above this energy. For the 1984 data we have included the range up to the last channel of the Xe data corresponding to an energy of 31 keV.

3. SPECTRAL MODELS

Cyg X-3 is a unique object that has been classified as a low-mass X-ray binary (LMXB), mainly due to its short orbital period (≈ 4.79 hr). Its spectral properties are also similar to those of other LMXBs and led White & Holt (1982) to propose an accretion disk corona (ADC) model for Cyg X-3. Observa-tions of Cyg X-3 in the infrared indicate a Wolf-Rayet (W-R) spectrum (van Kerkwijk et al. 1992) and a strong wind (~ 2000 km s^{-1}) that is optically thick (in infrared) to distances larger than the orbital separation is implied. This wind could be due to X-ray irradiation of either the accretion disk or a low-mass companion or alternatively could be completely intrinsic to the companion (van Kerkwijk et al. 1992). It has been shown, however, that accretion disks can form even in stellar wind–fed X-ray sources (Taam & Fryxell 1988; Fryxell & Taam 1988) and remain stable even under a vigorous mass loss (Melia et al. 1991). For the X-ray spectral analysis, we assume that, in Cyg X-3, the accretion onto the compact object is via an accretion
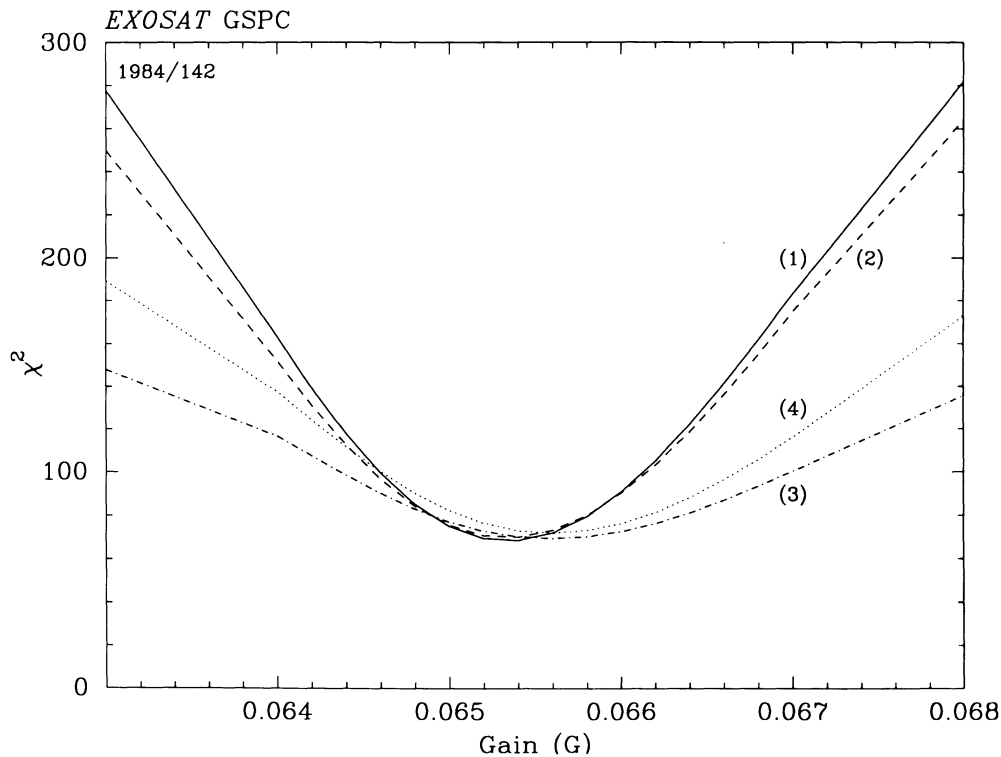
FIG. 3.—Values of χ^2 (dof-64) obtained by fitting the characteristic background lines in the *EXOSAT* GSPC detector, are plotted against the detector gain parameter (*G*) for the 1984/142 observations. Four consecutive spectral files with an integration time of ~5000 s were used for this analysis and they are numbered sequentially in the figure.

disk. The circumstantial evidence for this assumption comes from the detection of quasi-periodic oscillations in Cyg X-3 (van der Klis & Jansen 1985).

Simple spectral models like power-law, thermal bremsstrahlung, or blackbody have had little success in explaining good quality, broad-band X-ray spectra of X-ray binaries. A combination of at least two components has been quite satisfactory in fitting observed X-ray continuum from such sources. The preferred models for such combinations have been blackbody, various calculations of emission from accretion disks, and radiation resulting from the saturated Comptonization of low-energy photons by high-energy electrons in a plasma as calculated by Sunyaev & Titarchuk (1980). White, Stella, & Parmar (1988, hereafter WSP), have analyzed *EXOSAT* ME data from nine LMXBs of varying luminosities and have compared these data with various models of X-ray emission from an accretion disk surrounding a compact object in a binary system. They have tried various accretion disk models like the optically thick disk emission (multicolor blackbody) model (Mitsuda et al. 1984), modified blackbody disk emission model of Shakura & Sunyaev (1973) and also of Stella & Rosner (1984) and the Comptonization model of Sunyaev & Titarchuk (1980). A blackbody component was always included with the above models. WSP show that the Sunyaev & Titarchuk (1980) Comptonization model (hereafter referred to as the CompST model) in addition to a blackbody component gave the most reasonable fit to the spectra for all the objects considered. In fact two of the objects, XB 1608−52 and XB 1636−536, could not be fitted by any of the models other than the CompST model. In a subsequent study by Mitsuda et al. (1989), it was found that the spectrum of XB 1608−52 could be well

described by a model consisting of a multicolor blackbody spectrum expected from an optically thick accretion disk, and it was found to be marginally better than the CompST model.

In a few binary systems with suspected black hole companions, e.g., Cyg X-1, LMC X-3, and X1755−33, the thermal Compton model either by itself or in combination with a power-law model, has been most successful in characterizing their X-ray spectra (WSP; Done et al. 1992). In contrast, replacement of the thermal Compton model by emission from either the modified accretion disk models of Stella & Rosner (1984), where the viscosity scales with gas pressure, or that of Shakura & Sunyaev (1973), for the inner regions of the accretion disk where viscosity is dominated by radiation pressure, have not met with an equal degree of success.

The thermal Compton emission, therefore, has emerged as the best candidate for explaining either partly or wholly the X-ray spectrum of LMXBs and X-ray binaries suspected of harboring black holes. The thermal Compton emission is characterized by an electron temperature kT_e and an optical depth τ which together define the Comptonization parameter y $(=4kT_e\tau^2/m_ec^2)$. The geometry of the plasma cloud is unspecified and so is the origin of the cool photons, whereas the electron temperature is assumed to be constant. It could, however, arise from a corona in the inner accretion disk. Whenever a blackbody emission is detected in the spectra of low-mass X-ray binaries, it has been interpreted as the energy released from the boundary layer at the inner edge of the accretion disk, close to the heated surface of the neutron star with a low-magnetic field.

From the available spectral results on Cyg X-3, we can conclude that examining the X-ray spectra of Cyg X-3 in the light

of an accretion disk corona is a good starting point. To arrive at a generalized spectral model for Cyg X-3, we use the following guidelines:

1. The same model should give acceptable fits to both the "high"- and the "low"-state data.

2. The derived parameters should be physically meaningful.

3. The absorption due to neutral matter is likely to be the same for all the continuum components because these originate close to the inner accretion disk of the compact object.

4. It will be aesthetically pleasing (and a bonus) if the high-energy component can also explain the hard X-ray power-law emission measured from the balloon observations.

A summary of the various models and their parameters is given in Table 2.

4. ANALYSIS AND RESULTS

The spectral data were integrated for short durations of 0.2 binary phase, thus resulting in 11 spectral files for the 1983 data and six for the 1984 data. These spectral files will be referred to as the "binary phase spectra," for example, the spectra of binary phase 0.4 refer to the spectral data integrated from the binary phase 0.3 to 0.5 for the first binary cycle and the spectra of binary phase 1.4 refer to the data corresponding to the phase 0.3–0.5 in the second binary cycle and so on. Additionally, spectral files were also made by integrating data over one binary cycle (the phase-averaged spectral files). The phase-averaged spectra for the 1983 observation has been accumulated between the binary phases 1.3 and 2.3, and 1984 data are accumulated between the binary phases 0.5 and 1.5.

As the GSPC gain varied over the 1983 observations, appropriate response files were made for each of the binary phase spectral files, and the binary phases for the phase-averaged spectra were chosen such that the GSPC gain was stable over one binary cycle.

The observed PH spectra from the Ar and Xe half 1 arrays are shown in Figure 4 for the 1983 and 1984 phase-averaged data. The observed flux in 1983 (the "high state" of Cyg X-3) is a factor of 2 brighter in soft X-rays (Ar data) compared to the "low"-state flux in 1984. However, the hard X-ray flux (Xe data) are brighter in the "low" state. The apparent pivoting of the spectra near 10 keV may be influenced by the fact that at this energy, the Ar and Xe detectors have comparable efficiencies.

4.1. Progression toward the Generalized Spectral Model

Although it is likely, and indeed, as we see later, true, that at any given energy multiple components are present in the spectrum of Cyg X-3, we have taken the following simplified approach to arrive at a generalized model for the X-ray emission from Cyg X-3: (1) We first choose a limited energy range and make an appropriate choice of the most likely spectral component dominant in that energy range by spectral fitting and critically evaluating the resultant spectral parameters, and then (2) we choose another energy range and identify the next component and so on. Though we give the reasons for the choice of the energy region and the selection of the spectral components at every step, there is some element of subjectivity involved in these choices and also the order in which successive steps are taken. Nevertheless, we arrive at a statistically accept-

TABLE 2

SUMMARY OF MODELS USED IN THE SPECTRAL ANALYSIS

Model	Symbol	Parameter	Symbol	Units
Blackbody	bbody	Temperature	kT_{bb}	keV
		Radius	R	km
Power-law	pl	Photon index	Γ	...
		Normalization	K_{pl}	photons cm^{-2} s^{-1} keV^{-1}
Power-law with exponential cutoff	cutpl	Photon Index	Γ	...
		Cutoff energy	E_c	keV
		Normalization	K_{cp}	photons cm^{-2} s^{-1} keV^{-1}
Comptonization[a]	CompST	Electron temperature	kT_e	keV
		Opacity	τ	...
		Normalization	K	photons cm^{-2} s^{-1} keV^{-1}
Bremsstrahlung	br	Temperature	kT_{br}	keV
		Normalization	K_{br}	photons cm^{-2} s^{-1} keV^{-1}
Disk model[b]	diskm	Accretion rate[c]	$\dot{M}_m$	L_{edd}
		Inclination	K_m	radian
Disk model[d]	disko	Accretion rate[c]	$\dot{M}_o$	L_{edd}
		Inclination	K_o	radian
Gaussian	ga	Line energy	E_{line}	keV
		Line width	σ	keV
		Normalization	K_{line}	photons cm^{-2} s^{-1}
Absorption[e]	abs	Column density	N_H	cm^{-2}
Absorption edge	edge	Threshold energy	E	keV
		Absorption depth	τ_m	...

[a] Sunyaev & Titarchuk 1980.
[b] Stella & Rosner 1984.
[c] In units of accretion rate for Eddington luminosity.
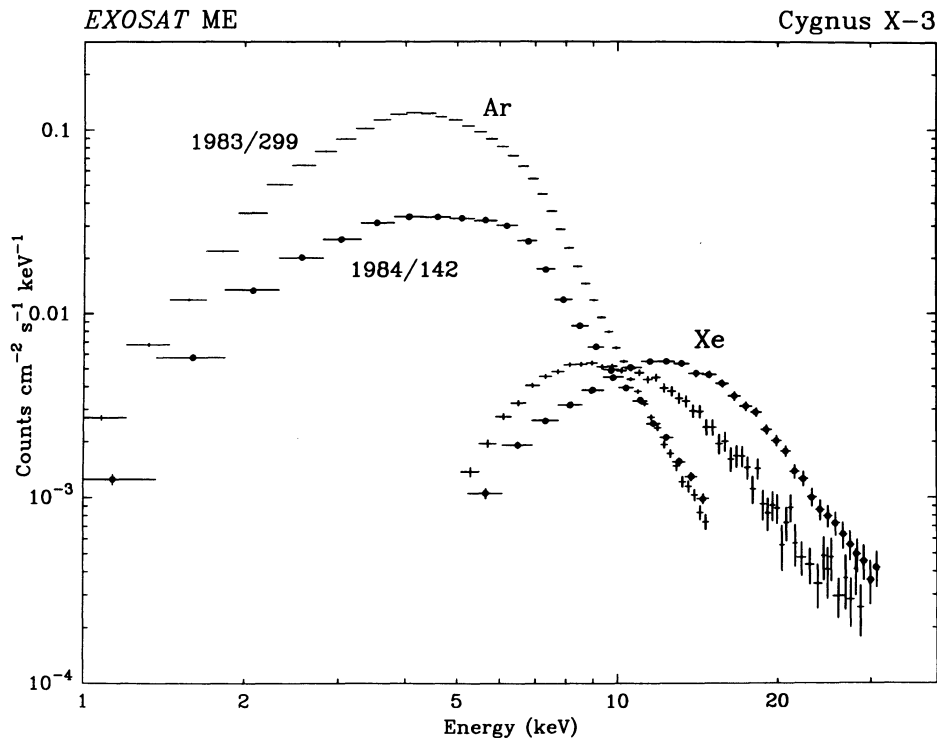[d] Shakura & Sunyaev 1973.
[e] Morrison & McCammon 1983.

FIG. 4.—Observed, binary phase-averaged, count rate spectra obtained from the *EXOSAT* ME argon (1–15 keV) and ME xenon (5–30 keV) detectors are shown for the "high" state (1983/299) and "low" state (1984/142) of Cyg X-3. The "high"-state data are shown as "plus" signs and the "low"-state data are shown as filled circles.

able spectral model which is sufficient to explain the complete spectra of Cyg X-3 in the 1–50 keV region for both the "high" and the "low" states, and it also agrees with the observations up to 100 keV. In a later section (§ 4.3) we argue that the final model arrived at is the simplest and most appropriate for Cyg X-3 and is not influenced by the method followed in the analysis.

It may be worthwhile to mention here the balancing act that we have performed throughout our analysis. The integration time of the spectral files has to be large enough to have sufficient signal-to-noise ratio, but not too large so as to corrupt the data by spectral evolution within the binary phase. As it turns out (see § 4.5) the range of variability of the spectral parameters within a binary cycle is much less compared to the parameter variation between the two states of the source. The eventual model is deduced by analyzing the phase-averaged data and verified by analyzing the phase-resolved spectral files, going back and forth at each stage. For reasons of clarity, we describe in the following subsections the method sketched above for the phase-averaged data, going to the phase-resolved spectral data whenever required, and indicating this explicitly. The successive spectral models that are fitted to the phase-averaged data, the energy range, the degrees of freedom (dof), and the resultant values of reduced minimum χ^2 (χ_v^2) are enumerated in Table 3, for the "high"- (1983 data) and "low"-(1984 data) states of Cyg X-3.

4.1.1. Low-Energy Continuum

The dominant component in the 3–5 keV region is modeled either as a blackbody (Serlemitsos et al. 1975; Sanford et al. 1975; Kitamoto et al. 1987; White & Holt 1982) or a power-law (Willingale et al. 1985), with neutral hydrogen absorption.

We have selected spectral data in this energy range from the Ar and GSPC detectors and attempted spectral fits using blackbody and power-law models with absorption, for the binary phase spectral files. The absorption coefficients given by Morrison & McCammon (1983) are used throughout. For the "high"-state data, the power-law model is slightly preferred over the blackbody, the improvement in χ_{min}^2 ($\Delta\chi^2$) being 18 for 38 dof, averaged over the individual binary phase spectral files. The blackbody, however, showed a strong preference over the power-law model for the "low"-state data, the average value of $\Delta\chi^2$ being 52 for 40 dof. Hence, we choose the blackbody as an appropriate model in the energy region of 3–5 keV.

4.1.2. High-Energy Continuum

Cyg X-3 has an intense line emission between 6 and 7 keV, and an absorption edge has been detected at ≈9.2 keV (Kitamoto et al. 1987). Therefore, we have ignored the energy region of 5–12 keV, temporarily, in order to identify, and model, the higher energy continuum. The lower energy region of 3–5 keV is covered by the Ar and GSPC detectors, whereas the energy region above 12 keV is covered by the Ar and Xe detectors. Modeling the energy region of 3–5 keV and >12 keV by just a blackbody with absorption results in unacceptably high χ_v^2 of 9.55 (for the "high" state) and 9.84 (for the "low" state). The residuals for the fit are shown in Figures 5a (1983 data) and 6a (1984 data). It can be seen that there exists a high-energy excess at >12 keV energy region, indicating the presence of a second continuum component. We have fitted the high-energy excess with the CompST model (Comptonization model of Sunyaev & Titarchuk 1980). Fitting with a blackbody and CompST model with a common absorption results in a χ_v^2 of 1.32 ("high" state) and 1.02 ("low" state) for 148 and 104

TABLE 3

PROGRESSION TOWARD THE GENERALIZED SPECTRAL MODEL

MODEL	ENERGY RANGE (keV)	1983/299		1984/142	
		χ_ν^2	dof	χ_ν^2	dof
abs1.bbody	3–5 and 12–20	9.55	151	9.84	107
abs1.(bbody + CompST)	3–5 and 12–20	1.32	148	1.02	104
abs1.(bbody + CompST + ga)	3–50[a]	2.85	259	2.00	212
abs1.edge1.(bbody + CompST + ga)	3–50[a]	2.20	257	1.69	210
abs1.edge1.edge2.(bbody + CompST + ga)	3–50[a]	1.10	255	1.30	208
abs1.edge1.edge2.(bbody + CompST + ga)	1–50[a]	2.45	266	1.31	220
abs1.edge1.edge2.(bbody + CompST + ga) + abs2.br	1–50[a]	1.23	263	1.29	219
abs1.edge1.edge2.(bbody + pl + ga) + abs2.br	1–50[a]	1.22	264	1.33	221
abs1.edge1.edge2.(bbody + cutpl + ga) + abs2.br	1–50[a]	1.24	263	1.28	220
abs.1.edge1.edge2.(bbody + br1 + ga) + abs2.br	1–50[a]	1.45	264	1.55	221
abs1.edge1.edge2.(bbody + disko + ga) + abs2.br	1–50[a]	1.24	264	1.55	221
abs1.edge1.edge2.(bbody + diskm + ga) + abs2.br	1–50[a]	1.24	264	1.58	221

[a] Upper limit is 31 keV for the 1984 data.

dof, respectively. Though the fit is reasonably acceptable, the spectral parameters are not well constrained due to the restricted energy range. We take CompST as a working model for the second continuum component and return to a critical evaluation of the different possible models for the high-energy component in a later section (§ 4.3).

4.1.3. Emission-Line and Absorption Edges

With the blackbody and CompST parameters determined above, we include the energy region of 5–12 keV. This energy region is covered by all the three detectors, the GSPC, Ar, and Xe. The residuals in the data for the complete energy region above 3 keV, after subtracting the spectrum due to the blackbody and CompST model parameters obtained above, are shown in Figures 5b ("high" state) and 6b ("low" state). The excess and a dip, in the residuals, indicate that there is an intense line emission and at least one absorption edge. Modeling the complete data above 3 keV with three additive models, viz., blackbody, CompST, a Gaussian line, and a common neutral absorption gives values of 2.85 (dof = 259) and 2.00 (dof = 212) for the χ_ν^2, in the "high" and "low" state, respectively. Inclusion of an absorption edge improves the χ_ν^2 to 2.20 and 1.69, respectively. The residuals to this fit are shown in Figures 5c ("high" state) and 6c ("low" state). The residuals for the "high" state indicate incorrect model fitting, particularly for energies between 6 and 11 keV. Further, we found it necessary to restrict the Gaussian line width (σ) to be <0.6 keV, for the "high" state, as allowing it free gives unrealistic values of Gaussian line energy (≈ 7.1 keV) and Gaussian line width (≈ 1.1 keV). Once we limit the σ to the above value, we get realistic values for line energy and width.

Inclusion of a second absorption edge improves the χ_ν^2 dramatically to 1.10 ("high" state) and 1.30 ("low" state). The $\Delta\chi^2$ is 283.97 and 85.40 for the "high" and "low" states, respectively, which justifies the inclusion of the second edge by a confidence level >99.99%, using the F-statistic. The energies of the two edges are ≈ 7.11 and ≈ 9.15 keV, respectively, for both the "states." For the "high" state, the line energy is restricted to be <6.95 keV, and for the "low" state, the absorption edge energy is restricted to be >7.1 keV.

The inference of the second edge is not influenced by any spectral evolution within the binary cycle. Including the second edge in the phase-resolved spectral files also improved the χ_ν^2 significantly. Average values of 91 and 50 are obtained for $\Delta\chi^2$, for the "high"- and "low"-state data, respectively. So we conclude that two edges are clearly preferred to a single edge.

4.1.4. Spectral Component below 3 keV

Having modeled the 3–50 keV emission from Cyg X-3, we attempted to model the soft emission below 3 keV that is believed to be external to Cyg X-3. We use only the Ar data in the energy range of 1–3 keV as it has the best sensitivity. When we lower the energy range to ≈ 1 keV and refit the data, with two common edges, a common low energy absorption to the three additive models, we get χ_ν^2 values of 2.45 ("high" state) and 1.31 ("low" state) for 266 and 220 dof, respectively. An examination of the residuals showed that there is a clear low-energy excess in the "high"-state data. We have modeled this excess as a thermal bremsstrahlung emission, with a separate neutral hydrogen absorption. The χ_ν^2 value now improves to 1.23 for the "high"-state data. The residuals of the fit to the "high"-state data are given in Figure 5d. We derive a value of $(9^{+7}_{-8}) \times 10^{-11}$ ergs cm^{-2} s^{-1}, in the 0.2–3.5 keV region for the observed flux from the thermal bremsstrahlung component. The errors reflect the uncertainty in the parameters. For the "low" state, this component is not needed, but using the parameters (temperature and N_H) obtained from the 1983 data, we derive a 90% confidence upper limit for the flux from the thermal bremsstrahlung component to be 4×10^{-11} ergs cm^{-2} s^{-1}. The residuals for the 1984 data in the 1–30 keV energy region are shown in Fig. 6d.

The ~ 0.3 keV thermal bremsstrahlung component could arise from the hot OB stars in the Cygnus OB2 association (White & Holt 1982). To estimate the contribution from the OB stars to the measured X-ray flux in ME, we have used the X-ray flux observed from these stars from the O-type star survey of the *Einstein Observatory* in the 0.2–3.5 keV region (Chlebowski, Harnden, & Sciortino 1989). From the position of these stars and the pointing of the ME detector, we have derived the expected flux incident on the detector as
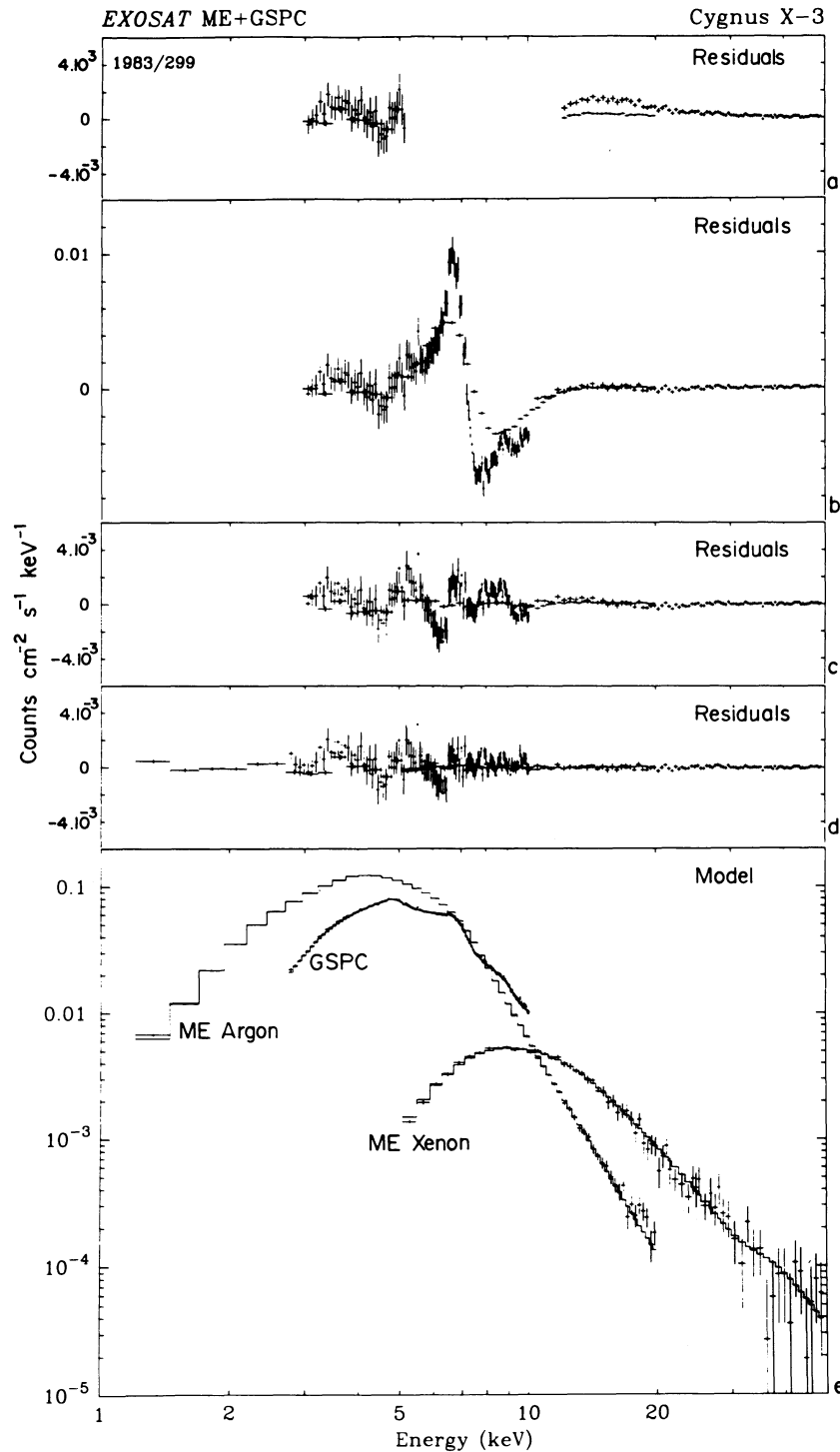
FIG. 5.—Residuals of the model fits to the data from *EXOSAT* ME argon, ME xenon and GSPC detectors, for various models tried at different energies for the "high"-state data of Cyg X-3 for one complete binary cycle (obtained on 1983/299). (*a*) Residuals to a single-blackbody fit in the energy range of 3–5 keV and >12 keV. (*b*) blackbody + CompST fits to the above energy range, but the residuals shown for >3 keV. (*c*) Residuals after adding a Gaussian line and an absorption edge. (*d*) Residuals for >1 keV after the addition of another absorption edge and a low-energy thermal bremsstrahlung component. (*e*) The observed count rate spectrum in the three detectors along with the final model folded through the detector response function shown as a histogram.
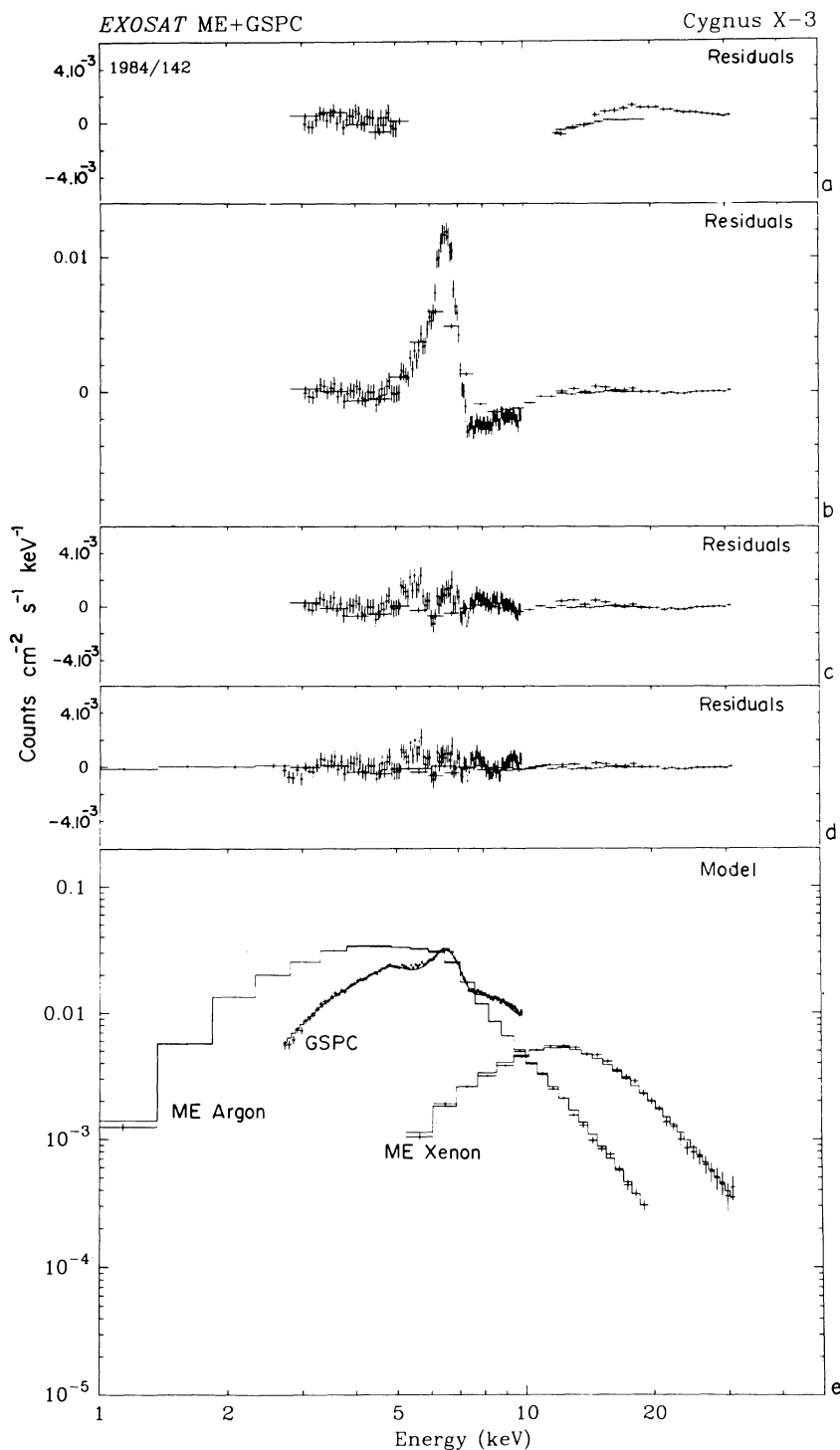
FIG. 6.—Same as Fig. 5 for the "low"-state data obtained on 1984/142. Thermal bremsstrahlung model below 3 keV was not required for the final model fit (6[d] and [e]).

$\approx 5.5 \times 10^{-11}$ ergs cm^{-2} s^{-1}. This agrees, within a factor of 2, with the observed flux in the low-energy component during the "high" state and the 90% confidence upper limit obtained for the "low" state of Cyg X-3.

It has been pointed out that the scattering of X-rays by interstellar grains (Mauche & Gorenstein 1986) could influence the spectral analyses of Cyg X-3 (Molnar & Mauche 1986). Molnar & Mauche (1986) have estimated the expected spectral shape of the scattered photons and found that it is similar to the ~ 1 keV blackbody emission and it has a factor of ~ 5 lower than the total intensity at >3 keV. Hence, the low-energy (~ 0.3 keV) component found in the "high"-state spectrum is most probably due to stars in the Cyg OB2 association. Since the spectral shape of the scattered photons is similar to the blackbody component, but lower in intensity (by about a factor of 5), it will have a marginal effect on the blackbody

parameters derived by us, but could influence some parameters such as N_H. The spectral parameters derived by taking data only above 3 keV are consistent with those derived by taking the complete energy range, but some parameters such as N_H are not well constrained. The identification of the low-energy component with its origin, or lack of it, does not affect the modeling of >3 keV emission from Cyg X-3.

4.2. The Best-Fit Spectral Model

The model that we have deduced consists of three additive models (blackbody, CompST, and a Gaussian line) modified by three multiplicative models (neutral absorption and two absorption edges). The 1983 "high"-state data also require an additional bremsstrahlung component with a separate neutral absorption. The observed count rate spectra are shown in Figures 5e ("high" state) and 6e ("low" state) for the Ar, Xe, and GSPC detectors. The fitted models, folded through the individual detector response functions, are shown as histograms. The adopted model fits the data quite well throughout the complete bandwidth of 1 to 50 keV (also see the residuals in Figs. 5d and 6d). As mentioned earlier, in the "low" state, the spectrum is harder and also the line feature in the 6–7 keV region stands out clearly.

The deconvolved spectra are shown in Figure 7 ("high" state) and Figure 8 ("low" state) for the binary phase-averaged spectra. The three additive models, modified through the multiplicative models, are shown separately, and the total model spectrum is shown as a histogram. For clarity, the unfolded data points are shown in a nonoverlapping manner such that Ar data covers 1–5 keV, the GSPC data 5–10 keV, and the Xe data >10 keV, though all the data points were

included (as described earlier) during fitting. It can be seen from Figures 7 and 8 that over most of the energy range more than one spectral component contributes significantly to the data.

Table 4 provides the parameter values of all the spectral components for the binary phase-averaged spectra. We also give the 90% confidence ranges on the parameters using χ^2_{min} + 4.61, keeping two closely associated parameters free. For example, in order to calculate the errors for the blackbody parameters, the rest of the model parameters are frozen except for the blackbody parameters and N_H. Similarly, while determining the errors in the line parameters, the rest of the model parameters are frozen except for the line parameters. The observed fluxes in the various spectral components (and also the fluxes without low-energy absorption) are given in the table. The total luminosity (distance = 8.5 kpc), in the energy region 1–50 keV changes from 10.6×10^{37} ergs s^{-1} to 6.2×10^{37} ergs s^{-1} in going from the "high" to the "low" state. The blackbody as well as the CompST luminosity decreased during the transition.

4.3. Evaluation of Other Spectral Models

We have obtained one of the most general spectral models for the X-ray spectra of Cyg X-3 that is statistically acceptable for both the "low"- and the "high"-state phase-averaged spectra. The eventual values of χ^2_ν are 1.23 and 1.29 for the "high" and "low" states, respectively, and they are further improved to ~ 1.1 when the phase-resolved spectral files are considered (see § 4.5). To establish the uniqueness of the model, we have attempted to fit some of the accretion disk models discussed in § 3 to the data, either as independent models or as
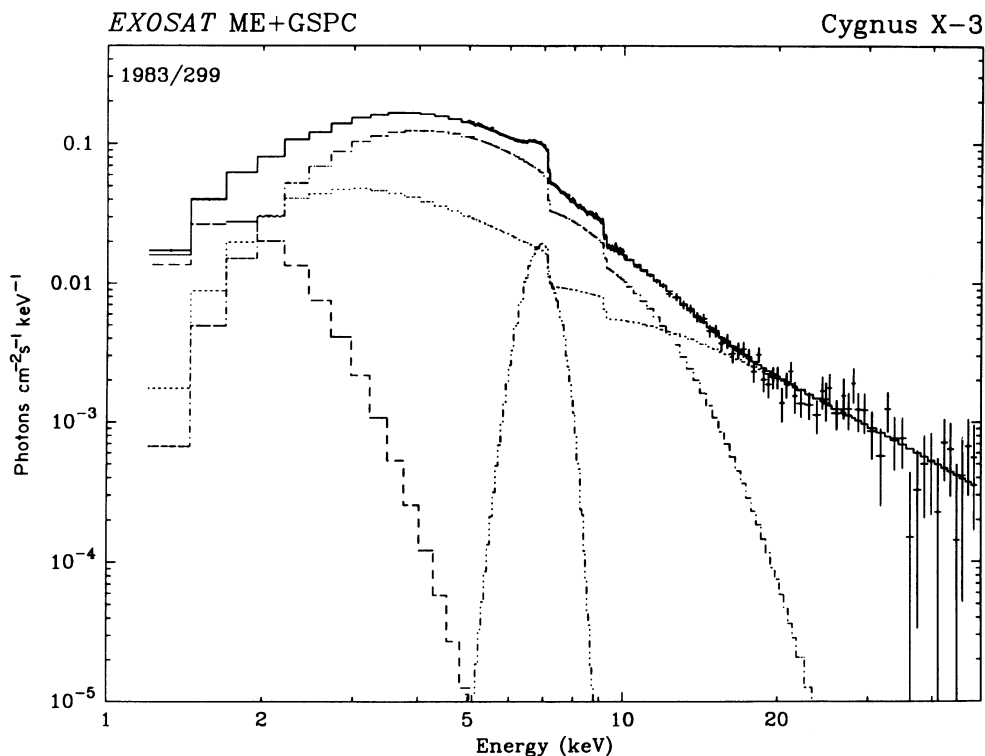

FIG. 7.—Deconvolved "high"-state spectrum of Cyg X-3, averaged over one binary cycle, obtained from the Ar, Xe, and GSPC detectors. For clarity, at a given energy, data from only one detector are shown. The contribution from the individual model components, blackbody ($kT_{bb} = 1.47$ keV), Gaussian line ($E_{line} = 6.95$ keV, $\sigma = 0.47$ keV), CompST ($kT_e = 27.5$ keV, $\tau = 3.2$), are also shown. These components are modified with the multiplicative models of neutral absorption ($N_H = 4.99 \times 10^{22}$ cm^{-2}) and two edges at 7.12 keV and 9.17 keV, respectively. A low-energy br component with a separate absorption is also shown in the figure.

EXOSAT ME+GSPC   Cygnus X-3
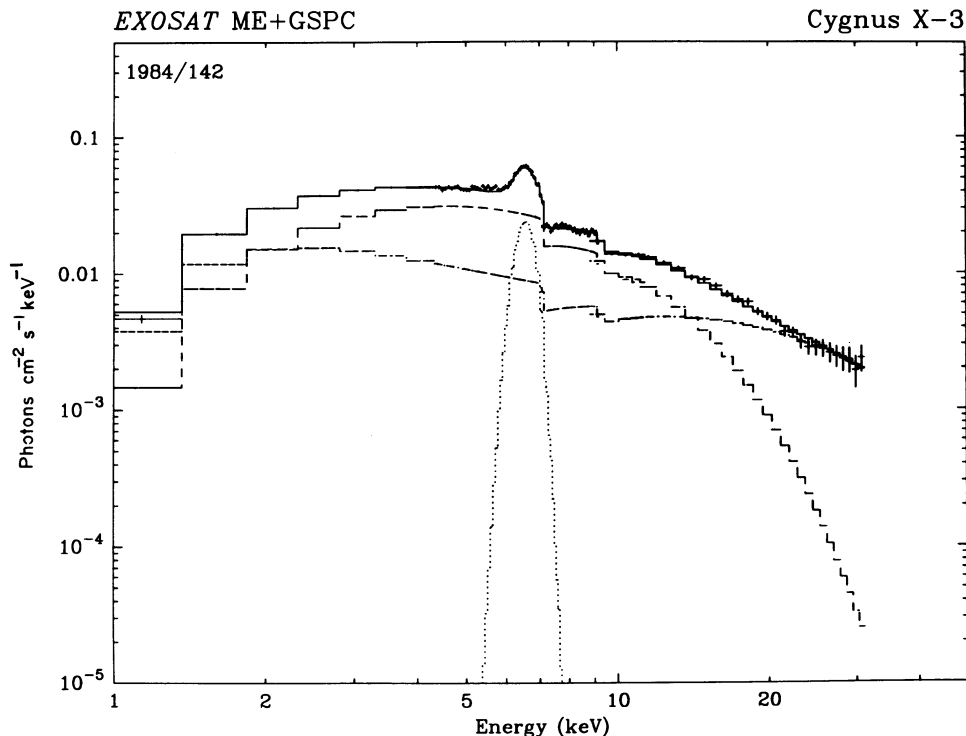

FIG. 8.—Same as Fig. 7, but, for the 1984/142 "low"-state data for Cyg X-3. The low-temperature thermal bremsstrahlung component is not required. The blackbody ($kT_{bb} = 2.40$ keV), line ($E_{line} = 6.56$ keV, $\sigma = 0.30$ keV), CompST ($kT_e = 7.8$ keV, $\tau = 15.5$) are shown separately, modified with neutral absorption ($N_H = 1.58 \times 10^{22}$ cm^{-2}) and two absorption edges at 7.10 keV and 9.12 keV.

a combination of models. We find that these models either fail to give an acceptable fit to the data or require parameters which are physically not meaningful. We have also critically examined some of the new results obtained by us, such as the two absorption edges, and find that these are not due to any bias in the data or any other artifact. A brief outline of these analyses is given below.

The models that we have used are thermal bremsstrahlung, power-law, power-law with an exponential cutoff, the disk model (disko) of Shakura & Sunyaev (1973), and the disk model (diskm) of Stella & Rosner (1984). None of these models could give acceptable fits to the data, when used independently (with or without the Fe line and absorption edges). We have used one of the above models as the second continuum component, in lieu of the CompST model, in the complete model described in the last section, and have refitted the data. The value of χ^2 for these models is given in Table 3. As the "low"-state data did not require the low-energy bremsstrahlung component, it is not included in the fit. We find that the use of thermal bremsstrahlung as the second component is ruled out because it gives an unphysical bremsstrahlung temperature for the "low"-state data (>500 keV). One of the accretion disk models, disko, does provide a good fit to the "high"-state data but requires an unusually large accretion rate, ~17 times the Eddington luminosity, to the "low"-state data. Therefore, disko, is also ruled out as it does not fit both the "low" and "high" states reliably. The other accretion disk model, diskm, provides accretion rates greater than 50 times the Eddington luminosity, for both the "high"- and "low"-state data and is again not a realistic model.

The power law also fits the 1983 and 1984 data quite well. However, the energy index (α) derived from the 1983 data is

≈ 1, whereas the 1984 data give a value of ≈ 0.1 for α. The latter index is flatter and overestimates the flux of photons at 100 keV, from Cyg X-3, by a factor of ~28 (Hermsen et al. 1987). Therefore, for the power law to explain the spectrum above 50 keV, a spectral cutoff at high energies is essential. The power-law model with a cutoff gives adequate fits to the data, and the spectral shape is quite similar to the CompST model. Moreover, we prefer the CompST model to a power-law with cutoff model because it is physically more meaningful (see § 3). Besides, cutoff power-law is an approximation for only unsaturated Comptonization.

We have also used the accretion disk models, disko and diskm, and the thermal bremsstrahlung model in lieu of the blackbody, in the complete model described by us. In the "low" state, the thermal bremsstrahlung model gives a χ^2_ν of 3.12, and for the "high" state it is >10. When we include disko, in lieu of blackbody, for the "low" state the χ^2_ν is 2.08 and for the "high" state, it is >10. However, the "low" state requires accretion rates that are 8 times that required for Eddington luminosity. When we include diskm, in lieu of blackbody, for the "low" state, the χ^2_ν is 2.78, and for the "high" state it is >10. However, the "low" state requires accretion rates that are 10 times that required for Eddington luminosity. We find, therefore, that the blackbody model, as the low energy component, is necessitated by statistical and physical considerations.

The existence of *the edge at* 7.1 keV *is being reported for the first time*, here. In ordinary proportional counters, the resolution is not sufficient to clearly isolate the edge feature from a broad line. It is the combination of high resolution of the GSPC, in which the edge can be seen as a sharp cutoff making the line appear asymmetric (Fig. 6c), with the ME,

TABLE 4

Model Parameters for Phase-Averaged Spectra

Model Component	Parameters	1983/299		1984/142[a]	
		Value	90% range[b]	Value	90% Range[b]
Model = abs1.edge1.edge2.(bbody + CompST + ga) + abs2.br					
abs2	N_H (10^{22} cm^{-2})	3.8	(2.7, 5.0)	[a]	[a]
br	kT_{br} (keV)	0.38	(0.32, 0.47)	[a]	[a]
	K_{br}	47.4	(10.4, 250.0)	[a]	[a]
abs1	N_H (10^{22} cm^{-2})	4.99	(4.97, 5.01)	1.58	(1.52, 1.65)
bbody	kT_{bb} (keV)	1.470	(1.467, 1.473)	2.40	(2.38, 2.42)
	R (km)	10.34	(10.29, 10.39)	2.53	(2.50, 2.57)
CompST	kT_e (keV)	27.5	(13.1, ∞)	7.8	(7.35, 8.34)
	τ	3.2	(<5.0)	15.5	(14.9, 16.0)
	K	0.916	(0.902, 0.931)	0.065	(0.063, 0.067)
	y	2.20	...	14.67	(14.49, 14.73)
ga	E_{line} (keV)	6.950	(6.928, 6.975)	6.555	(6.533, 6.576)
	σ(keV)	0.47	(0.44, 0.51)	0.30	(0.26, 0.34)
	K_{line}	0.0247	(0.0240, 0.0254)	0.0183	(0.0176, 0.0190)
	EW (eV)	296	(281, 311)	494	(469, 519)
edge1	E_1 (keV)	7.12	(7.10, 7.13)	7.10	(7.05, 7.15)
	τ_{m1}	0.495	(0.487, 0.503)	0.448	(0.430, 0.467)
edge2	E_2 (keV)	9.17	(9.10, 9.23)	9.12	(9.02, 9.22)
	τ_{m2}	0.35	(0.33, 0.37)	0.31	(0.28, 0.34)
χ^2_ν(dof)		1.23 (263)		1.29 (220)	
Fluxes[c] (10^{-9} ergs cm^{-2} s^{-1})					
bbody	...	5.3 (7.4)		3.0 (3.2)	
CompST	...	3.8 (5.6)		4.4 (4.5)	
Total	...	8.5 (12.2)		6.9 (7.2)	

[a] 1984 data do not require the additive model abs2.br.
[b] χ^2_{min} + 4.61 with two free parameters.
[c] Total and CompST flux was derived over 1–50 keV. Figures in brackets have been corrected for low-energy absorption.

which can fix the continuum very well due to its high sensitivity and large bandwidth of 1–50 keV, that we have been able to isolate the 7.1 keV edge. Without the second edge, residuals in the ME Ar and GSPC data showed residuals with opposite trends (positive and negative), indicating an unmodeled feature in the source spectrum. Approximating a sharp feature by a smooth function will produce such trends in the residuals for detectors with significantly different energy resolution. This also explains why the absorption edge at ≈ 7.1 keV could have been missed in the *Tenma* observation (Kitamoto et al. 1987).

We have also made sure that two edges are necessarily required even when different combinations of the continuum and absorption models (which are allowed by the χ^2 test) are adopted. A cutoff power law in lieu of CompST gave similar results, with values of $\Delta\chi^2$ when the 7.1 keV edge is added being 188 and 109, for the "high" and "low" states, respectively. Different combinations of the components, e.g., using separate N_H for the continuum components, not using any multiplicative models for the Gaussian line, etc., also required a second edge and did not make any significant change in the derived parameters.

4.4. Results from Phase-averaged Spectra

4.4.1. Blackbody Component

The blackbody component shows a dramatic change as the source transits from a "high" to a "low" state. The temperature increases from 1.5 keV to 2.4 keV, and the equivalent radius of the blackbody emission region decreases from 10.3 km to 2.5 km. These observations imply a very compact emission region for this component. Its contribution to the total luminosity is significant throughout, although it decreases from 0.61 in the "high" state to 0.44 in the "low" state.

4.4.2. High-Energy Component

The CompST component is the major contributor to the X-ray continuum in the "low" state. The parameters show a significant difference between the two intensity states of Cyg X-3, even though in the "high" state the data do not constrain the parameters too well. It is, however, quite certain that the electron temperature (kT_e) is higher, whereas the opacity (τ) is lower in the "high" state. The parameters are well determined in the "low" state and imply a highly saturated Comptonization with y in the region of 15. The value of y in the "high" state is ~ 2.2.

Previous spectral measurements above 20 keV have not shown any long-term variability, and all the measurements agree with each other correct to 10%–30% (Hermsen et al. 1987; Rao et al. 1991). It is instructive to compare the extrapolated CompST model derived above for the two states of Cyg X-3 with the measured spectrum above 20 keV. The CompST models derived for the "low" state are shown in Figure 9 (*hatched region*) after extrapolation to 100 keV, for the 90%
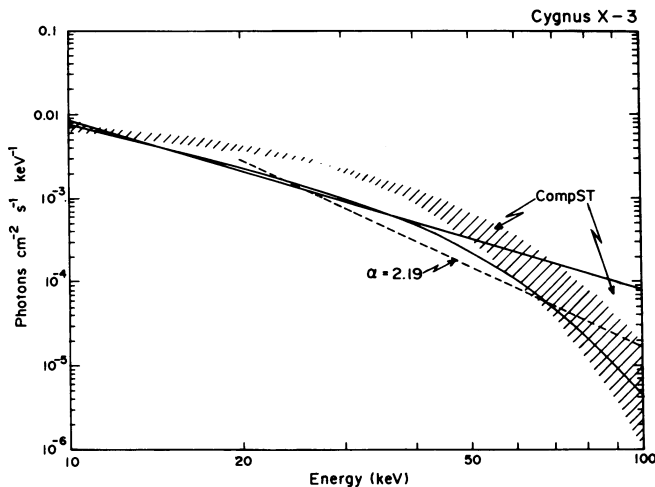
FIG. 9.—Extrapolation to 100 keV of the 90% confidence range of CompST model parameter, kT_e, obtained for the "low"-state data is shown as a hatched region. The extrapolated bounds on CompST emission, obtained from the best-fit parameter and the 90% confidence lower limit on kT_e, are shown as solid lines for the "high"-state data. The power-law spectrum (energy index $\alpha = 2.19$) obtained from balloon observations (Hermsen et al. 1987) is shown as a dashed line.

confidence range of CompST parameter, kT_e. Since the "high"-state values of kT_e are not well constrained (see Table 4), the best-fit parameter and the parameter corresponding to the 90% confidence lower limit on kT_e are shown in Figure 9 (continuous lines). The power-law model fitted to the X-ray spectrum above 20 keV (Hermsen et al. 1987) is also shown in Figure 9 (dashed line). It can be seen that the CompST model derived for the "high" state agrees, within a factor of 2, with the power-law spectra derived from the hard X-ray observations. Considering the fact that these two models are derived for the data obtained from two different detectors at different times, this agreement can be treated as satisfactory.

The CompST model derived for the "low" state also agrees with the hard X-ray data above 50 keV. Between 20 and 50 keV, they disagree by a factor of ∼4. Since the "low" state is relatively infrequent, it is possible that the hard X-ray spectral results were obtained only in the "high" state. It will be extremely useful to obtain the hard X-ray spectra of Cyg X-3 in its "low" state. All the models derived so far for Cyg X-3 based on the low-energy data are not consistent with the steep power law observed in hard X-rays. The spectral model derived here naturally explains a steep power-law in the hard X-rays, though disagreeing in the finer spectral details at 20–50 keV for the infrequently seen "low"-state data.

4.4.3. Line Features

Cyg X-3 is an extremely bright source of the Fe line. The line has been detected at 6.56 ± 0.03 keV in the "low" state and ∼6.95 keV in the "high" state, both significantly higher than expected from the fluorescence of cold iron. The measured line positions imply that in the "low" state the iron must be ionized to at least Fe XX (N-like), and in the "high" state almost to Fe XXVI (H-like). The ionization parameter, ξ, therefore must be close to 100 in the "low" state and ≥ 1000 in the "high" state (Kallman & McCray 1982). Therefore, if these lines originate due to fluorescence, then the line-emitting region must be highly or fully ionized. The line has a measurable width. In the "high" state, the line width, σ, is 0.5 keV (FWHM = 1.1 keV). For the "low" state, however, the line

width is indicated to be somewhat narrower with $\sigma = 0.3$ keV (FWHM = 0.67 keV). The line flux is ∼30% higher in the "high" state, and the equivalent width (EW) of the line is 300 eV. The corresponding value for the EW in the "low" state is 500 eV.

The edge energy of 7.1 keV corresponds to absorption by cold iron. The value of maximum absorption depth (τ_{m1}) is 0.50 in the "high" state and 0.45 in the "low" state. A second edge at 9.2 ± 0.1 keV is detected in both the intensity states of Cyg X-3. The value of maximum absorption depth (τ_{m2}) is 0.35 in the "high" state and 0.31 in the "low" state. For the second edge, the energy is closer to the value of 9.3 keV expected from absorption by Fe XXVI than 8.8 keV for Fe XXV. The edge energy and τ_{m2} are mutually consistent between the "low" and "high" states, within 90% confidence. This implies the existence of highly ionized absorbing medium with $\xi \geq 1000$ in both the intensity states.

The values τ_{m1} and τ_{m2} are used to derive the column density of the absorbing iron. The photoelectric absorption cross section is 3.8×10^{-20} cm^2 atom^{-1} for cold iron and 3.3×10^{-20} cm^2 atom^{-1} for Fe XXVI (see George & Fabian 1991). Using these values we estimate a column density of Fe I to be in the range $1.3–1.4 \times 10^{19}$ cm^{-2} and column density of Fe XXVI to be $1.0–1.1 \times 10^{19}$ cm^{-2}, which are comparable. For normal solar abundance of iron (3.3×10^{-5}) the equivalent column density of the absorbing matter (N_H) is $3–4 \times 10^{23}$ cm^{-2} which is nearly 7–8 times more than the highest value seen in the low-energy absorption in the "high" state. If the low-energy absorption and the 7.1 keV edge are produced by the same matter, then either an overabundance of iron or a very special geometrical constraint is needed.

4.5. Variation of Spectral Parameters with Binary Phase

The reasonably good fit obtained for the binary phase-averaged data indicates that there are no dramatic variations in the spectral parameters within the binary cycle. To identify the spectral parameters that are varying with the binary phase, we have analyzed the phase-resolved spectral files, each of duration corresponding to 0.2 orbital phase. To avoid any possible complications arising from the dust-scattering effects (Molnar & Mauche 1986), we have analyzed data only above 3 keV. The number of spectral bins involved in this analysis are 267 for the "high" state and 220 for the "low" state.

Using the spectral parameters obtained from the analysis of the phase-averaged spectra, we have fitted the phase-resolved spectral files by allowing only the normalization of the continuum components to vary. We obtain, on an average, a value of χ_ν^2 of 2.7 for the "high" state and 1.6 for the "low" state. Considering that the observed signal-to-noise ratio in each spectral bin is about 100, the derived values of χ_ν^2 imply that >98% of the observed flux can be explained by the variations in the normalization constants of the continuum components only. Allowing the N_H to vary further improved the average χ_ν^2 to 1.25 ("high" state) and 1.24 ("low" state). Since the observed N_H has negligible effect above 5 keV, we can conclude that most of the binary variations above 5 keV can be explained by the variations in the normalization of the continuum parameters only.

By varying the parameters of absorption (τ_{m1} and τ_{m2}), we obtain, on average, values of χ_ν^2 ∼ 1.19 and 1.15, for the "high" and "low" states. The absorption edge energies are held fixed at the values obtained from the phase-averaged analysis, as they are the same even in the two "states" and therefore will

TABLE 5

Best-Fit Parameters for Phase-resolved Spectra

PHASE	abs1 N_H $(10^{22}$ cm$^{-2})$	bbody kT_{bb} (keV)	R (km)	Flux[a] 1	Flux[a] 2	CompST Flux[a] 1	CompST Flux[a] 2	LINE Flux[a]	EW[b] (eV)	EDGES τ_{m1}	τ_{m2}	χ^2_ν
					1983/299							
0.2	5.88	1.52	9.34	4.94	7.00	3.83	5.61	0.237	255	0.59	0.46	1.02
0.4	4.80	1.51	10.03	5.80	7.88	3.30	4.70	0.282	287	0.60	0.35	1.07
0.6	4.50	1.42	13.33	7.77	10.78	4.08	5.76	0.336	265	0.46	0.27	1.28
0.8	4.05	1.46	9.73	4.78	6.39	3.06	4.26	0.342	429	0.48	0.23	1.13
1.0	4.66	1.67	6.06	3.32	4.28	2.51	3.55	0.263	447	0.68	0.48	1.10
1.2	5.25	1.52	9.05	4.75	6.55	3.45	4.98	0.238	277	0.56	0.42	1.10
1.4	5.00	1.52	10.25	6.04	8.28	4.22	6.05	0.284	265	0.55	0.36	1.16
1.6	4.85	1.41	13.36	7.46	10.55	5.09	7.26	0.301	232	0.43	0.30	1.02
1.8	4.23	1.40	11.65	5.57	7.69	3.73	5.22	0.267	286	0.40	0.27	1.07
2.0	4.46	1.63	6.64	3.57	4.61	2.39	3.37	0.291	474	0.63	0.48	1.00
2.2	5.00	1.53	9.00	4.80	6.55	3.18	4.56	0.258	306	0.58	0.41	0.92
Average	4.79	1.51	9.86	5.35	7.32	3.53	5.06	0.282	320	0.54	0.37	1.08
rms	0.51	0.09	2.33	1.40	2.06	0.78	1.08	0.035	86	0.09	0.09	0.09
Typical error[c]	0.25	0.02	0.10	0.10	0.10	0.40	0.40	0.027	30	0.03	0.07	
					1984/142							
0.6	1.65	2.30	2.97	3.45	3.69	6.35	6.55	0.237	484	0.44	0.29	1.05
0.8	0.87	2.27	2.53	2.43	2.53	4.72	4.82	0.193	559	0.39	0.27	1.17
1.0	0.76	2.55	1.73	1.82	1.88	3.12	3.18	0.156	690	0.37	0.31	0.98
1.2	1.91	2.60	2.46	3.86	4.09	3.55	3.68	0.169	404	0.53	0.42	1.06
1.4	1.15	2.58	2.71	4.68	4.87	3.73	3.82	0.178	365	0.53	0.47	1.17
1.6	0.56	2.55	2.84	4.96	5.07	3.41	3.46	0.225	445	0.51	0.47	1.25
Average	1.15	2.48	2.54	3.53	3.69	4.15	4.25	0.193	491	0.46	0.37	1.11
rms	0.53	0.15	0.44	1.23	1.27	1.21	1.26	0.032	118	0.07	0.09	0.09
Typical error[c]	0.40	0.08	0.05	0.01	0.01	0.45	0.45	0.014	35	0.04	0.07	

NOTE.—Model applied to the data is abs1.edge1.edge2.(bbody + CompST + ga). The line parameters (E and σ), CompST parameters (kT_e and τ), and the absorption edge energies (E_1 and E_2) are not displayed as they were frozen at the phase-averaged values. The degrees of freedom are 261 (1983 data) and 214 (1984 data).

[a] Blackbody, CompST (1–50 keV), and line flux have units of 10^{-9} ergs cm^{-2} s^{-1}. Col (1) corresponds to observed flux, whereas col. (2) corresponds to flux values corrected for low-energy absorption.

[b] EW: equivalent width.

[c] $\chi^2_{min} + 4.61$.

not change within a binary phase. In addition, allowing the blackbody temperature (kT_{bb}) to vary improved the χ^2_ν to about 1.08 and 1.11. The effect of varying all the other six parameters is to improve the χ^2_ν to 1.03 and 1.06. This improvement (average value of $\Delta\chi^2$ being 19) does not warrant the inclusion of these additional six parameters because a value of $\Delta\chi^2$ of 3.84 is required to include an additional component at a confidence level of 95% (using the F-statistic). An examination of the derived values of the parameters when all the 13 parameters are varied, while fitting, showed that some of the parameters are, in reality, constant (line energy and absorption edge energies) and some parameters showed marginal variation due to their close coupling with some other parameters (kT_{bb} vs. kT_e and σ vs. τ_{m1}). Hence, we present the binary phase-resolved spectra based on an analysis where seven parameters (the three normalizations of the continuum components, the three absorption parameters, and kT_{bb}) are allowed to vary. We have also carried out the phase-resolved spectral analysis in finer phase bins (0.05) with similar results, but the parameters are not well constrained due to larger statistical errors.

The spectral parameters determined for the different binary phases are displayed in Table 5 for both the "high"- and "low"-state observations. The fluxes observed and corrected for low-energy absorption for the various additive spectral components are also given in Table 5. The mean value of the

parameters, the rms variation in them, and the typical 90% confidence ranges (obtained by $\chi^2_{min} + 4.61$, keeping all the parameters free) are also given in Table 5.

Plots of some important spectral parameters across the binary phase are shown in Figures 10 and 11 for the "high" (open circles) and the "low" state (filled circles) of Cyg X-3 along with the 90% errors. The fluxes in the continuum models, corrected for the low-energy absorption, are shown in Figure 10, along with the equivalent width (EW) of the Fe line emission. The variation of the parameters kT_{bb}, N_H, τ_{m1}, and τ_{m2} with the orbital phase are shown in Figures 11a, 11b, 11c, and 11d, respectively.

The continuum fluxes show, as expected, variations correlated with the light curve variations, the maxima occurring at phase 0.6 and the minima at 0.0. The blackbody flux shows maximum modulation with the orbital phase. The modulation depth, defined as (maximum − minimum)/maximum, is 56% in the "high" state and 49% in the "low" state. The modulation depth for the blackbody component increases to 75% and 66% for the two states, respectively, if only the blackbody normalization is considered. The modulation depth of the CompST flux (36%–47%) compares well with the modulation depth of 41% observed between 20 and 40 keV from the balloon observations (Hermsen et al. 1987). A modulation depth of ~32%, in the line flux, is seen in the "low" state. The measured line
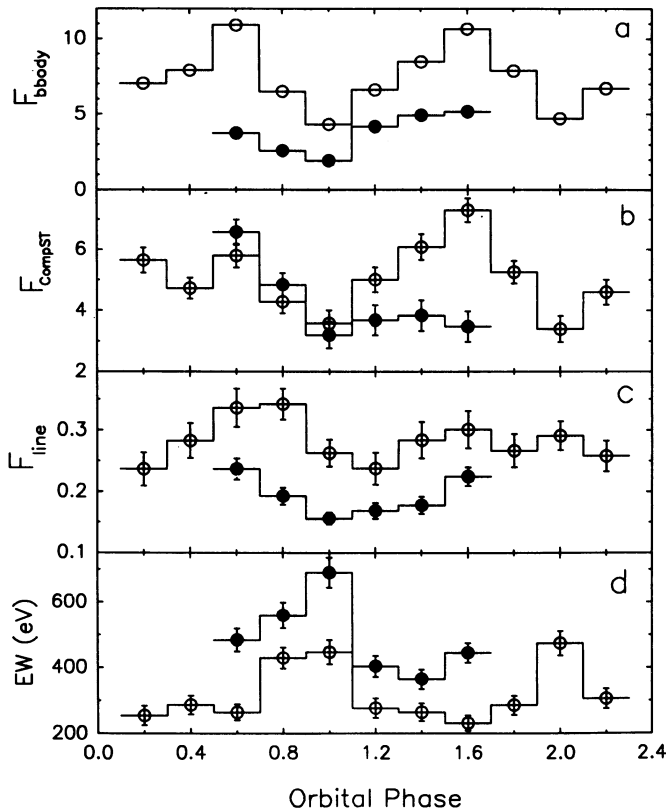
FIG. 10.—Plot of bbody (a), CompST (b), and Fe line (c) fluxes, corrected for low-energy absorption, with respect to the orbital phase. Also shown is the equivalent width of the line (d). The open circles represent the "high"-state data, while the filled circle represent the "low"-state data. The 90% confidence (χ^2_{min} + 4.61) errors are also shown, when they are larger than the symbols. Fluxes are in units of 10^{-9} ergs cm^{-2} s^{-1}.

FIG. 11.—Plot of kT_{bb} (a), N_H (b), τ_{m1} (c), and τ_{m2} (d) with respect to the orbital phase. N_H is in units of 10^{22} cm^{-2}. Symbol and error styles are like those in Fig. 10.

fluxes have larger errors in the "high" state, but the modulation depth is consistent with that derived for the "low" state.

The equivalent width of the iron line emission and the absorption edge depths show similar tendencies, with the minima occurring in a broad range between orbital phases 0.2 and 0.6 and the maxima peaking at phase 0.0. The variation of the EW is similar to that reported by Willingale et al. (1985). All the three parameters (EW, τ_{m1}, τ_{m2}) have modulation depths of 30%–50%. The blackbody temperature and N_H do not show any significant variation in the "low" state. In the "high" state these parameters show a shallow (10%–20%) modulation, which is repeated over two binary cycles. There is an indication that the N_H peaks slightly later than kT_{bb}.

5. DISCUSSION

We have arrived at one of the simplest spectral models for Cyg X-3, with a minimum number of parameters, that is statistically acceptable. It is sufficiently general as it explains the 3–50 keV spectrum of Cyg X-3 in both the "low" and "high" states and across the binary phase and, on extrapolation, explains the X-ray emission up to 100 keV. We interpret and discuss the various components of its emission and absorption below.

5.1. Continuum X-Ray Emission

The X-ray continuum in the spectra of Cyg X-3 consists of a combination of X-ray emission from a blackbody and a Comp-
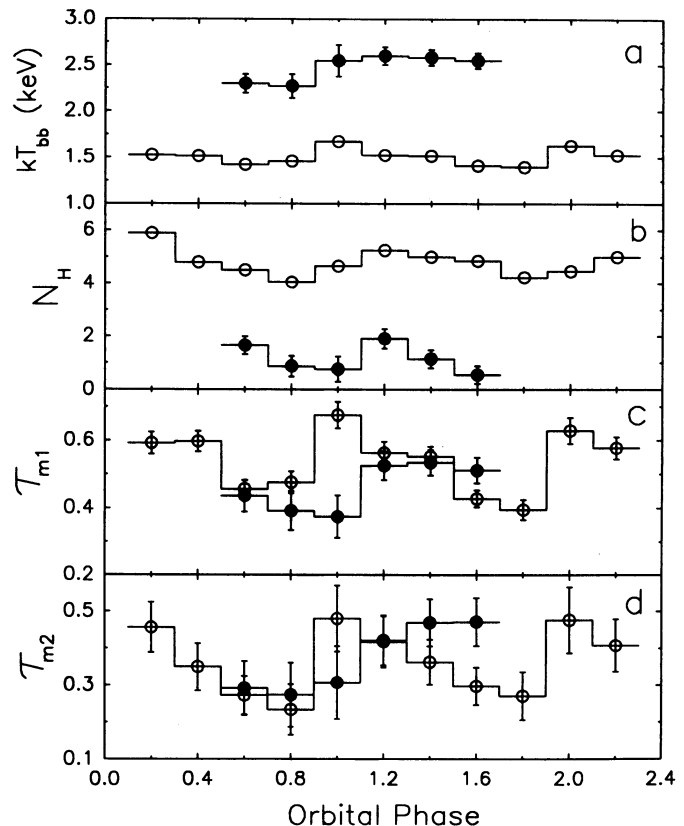
tonized plasma, which is similar to the results obtained on several LMXBs (WSP). Extending this analogy, we can conclude that the source of X-ray emission in Cyg X-3 is an accretion disk. We discuss the results obtained within this framework. As discussed earlier (§ 3), an accretion disk can form even in the presence of strong stellar wind.

The blackbody flux has the maximum modulation depth of all the spectral components (see § 4.5). This fact coupled to its compact size and high temperature implies it most probably originates very close to the surface of the compact object in the binary system, e.g., the boundary layer between the neutron star surface and the inner region of the accretion disk or the innermost region of the accretion disk itself. Its luminosity is then very sensitive to the mass accretion rate from the companion star. The variability of blackbody flux with phase (Fig. 10) shows sharply defined peaks near the phase 0.0 and 0.6, thereby restricting the inclination angle for the outer disk and the orbital plane containing the companion star with respect to our line of sight. A near edge-on situation in which the disk and the star occult the blackbody partially is not ruled out. As has been found by previous workers, the variability does not appear to be linked to absorption by cold matter as the N_H shows very little modulation and is maximum near 0.2 phase, whereas the F_{bb} is minimum at 0.0 phase. The blackbody temperature shows a mild but significant modulation only in the "high" state.

The kind of variation, between the "low" and "high" states described above, in the blackbody component (kT_{bb} and luminosity) is similar to that found in the high-luminosity

system XB 1820−30, except that the fraction of the black-body flux to the total flux varied in the opposite sense (WSP). In this system the blackbody component had a temperature ≈ 2.4 keV in the "low" state and ≈ 2.0 keV in the "high" state. Similar blackbody temperatures with large variations in them are also seen in the quiescent state of Sco X-1 (White, Peacock, & Taylor 1985). In another high-luminosity system, GX 349+2 (also known as Sco X-2), that exhibits "low" and "high" states, the variation in the blackbody temperature was in the opposite sense to that observed in Cygnus X-3 and XB 1820−30 (WSP).

The CompST component of the model can easily be extrapolated to explain its observed spectrum over a wider range of energies up to 100 keV. It shows smaller modulation depth than the blackbody component, and we place its origin a little further away from the source in an ionized region, e.g., a coronal region in or around the two-temperature accretion disk (Shapiro, Lightman, & Eardley 1976). The derived value of kT_e in the "high" state is higher than any of the sources listed by WSP and is more like the values found in Cyg X-1 (Done et al. 1992). The derived values of τ (Table 4) indicate that this region is more extended in the "high" state and/or more compact in the "low" state. The change of CompST parameters from "high" to "low" state may imply a transition from a two-temperature thick disk (high kT_e, low τ) corona to a thin disk (low kT_e, high τ) corona, probably associated with a decrease in the overall luminosity due to a reduction in the accretion rate.

A common absorbing matter for the low-energy X-rays is found to be adequate for the two components of the continuum. In the "low" state, the derived value for N_H is consistent with the lower limit of $1.4–1.7 \times 10^{22}$ cm^{-2} from the 21 cm measurements (Laeque, Lequeux, & Rieu 1972; Chu & Bieging 1973). Therefore, it would be ideal to observe Cyg X-3 in the optical–near-infrared when it is in the "low" state. There is no significant modulation seen in N_H in the "low" state, but a mild modulation is observed in the "high" state. These results imply that the low-energy absorption intrinsic to the source is present only in the "high" state. This could partly be a result of the expanded CompST region in the "high" state.

One of the interesting results obtained here is that the binary variation of the source intensity can be explained, almost entirely, by the variations in the normalization constants of the continuum components. The value of N_H obtained in the "low" state is comparable to the interstellar neutral N_H, indicating that there is little neutral matter in the binary system to cause any systematic variation. The value of the modulation depth does not change when the absorption effect is taken into account (see Table 5), both for the "high" and the "low" states. Hydrodynamic simulations of the stellar wind fed X-ray binaries show that the absorption effect is significant even for very high X-ray luminosities ($> 10^{37}$ ergs s^{-1}) (see Blodin et al. 1990). The absence of absorption effect in Cyg X-3 does not make the stellar wind model very attractive even though it has been used in the past to qualitatively explain the binary modulation of the X-ray flux from Cyg X-3 (Willingale et al. 1985).

In the present study we find that a spectral model in the framework of an accretion disk corona gives a very satisfactory fit to the data. Further, the geometric location of the spectral components based on the ADC model (see § 5.4) indicates a relatively stable accretion disk, which is contrary to the stellar wind model. From the available observations, it can be concluded that Cyg X-3 is an unique object, and much work remains to be done on the interaction of radiative heating,

radiation pressure, and wind dynamics around a low magnetic field neutron star. The present study strongly indicates the presence of a stable accretion disk around the compact object. To develop a refined geometric model, one needs precise measurements of the spectral parameters, which can be obtained by folding data over several binary cycles. Spectrally resolved timing analysis to look for lag, etc. (like the one reported by Kitamoto et al. 1992) will also help to localize the continuum components in the binary system. Such a detailed analysis is beyond the scope of the present paper.

5.2. Iron Line Emission

The iron line emission is detected from a highly ionized region which is almost fully ionized in the "high" state. The line flux is not very different in the two states, but the equivalent width is significantly different. Similarly, the line flux shows very little modulation depth, but the equivalent width shows almost the same modulation as the CompST component. The variation of the EW with phase is identical to that reported earlier by Willingale et al. (1985). These results imply that the line responds mostly to the changes in the continuum of the X-ray source and to the number of photons available above the K-edge of the iron. The line emission, therefore, can arise due to fluorescence of the ionized matter at a distance more removed from the central source than the CompST region.

The line is almost as wide as reported earlier by White & Holt (1982) for Cyg X-3, and by White et al. (1986) for many LMXBs. The observed widths cannot arise due to thermal Doppler broadening. Large widths can arise due to the effects of line blending and Comptonization due to electron scattering in the plasma (Kallman & White 1989). The line widths can thus provide information about the temperature and the optical depth of the fluorescing matter. These effects, however, also cause the line energy to shift to lower energies. Using the results of Kallman & White (1989) we find that to produce the observed width of the Fe line the optical depth of the scattering region has to be smaller than the τ found for the hot Comptonized region responsible for the high-energy continuum. The observed line energy of 6.95 keV in the "high" state puts an even more stringent limit on the optical depth, as the allowed shift would have to be negligible. Second, the value of the ionization parameter used by Kallman & White (1989) is higher than the value quoted above based on line energy, particularly, in the "low" state, although higher values of ξ are not ruled out by the data as is shown from the presence of 9.2 keV absorption edge in the "low" state. The line emission, therefore, occurs either in a very thin layer on the outside boundary of the "thick" Comptonized region or in a much thinner and possibly cooler scattering region.

All the above facts point to the possibility that the line originates in an accretion disk around the compact object by intercepting a large amount of the X-ray flux scattered from the continuum source (largely CompST region), as was pointed out by White et al. (1981) for the case of 4U 1822−37. Kallman & White (1989) used simplified model of an accretion disk, with respect to the ADC, in interpreting the properties of the iron line. The more sophisticated versions of the ADC model predict an inner disk of low ionization, a thin zone of intermediate ionization, and highly ionized iron (Fe xxv and Fe xxvi) above (Vrtilek, Soker, & Raymond 1993). Monte Carlo simulations of this advanced model of ADC indicate that the line strength and the large equivalent width of Cyg X-3 could be due to geometry. To produce the measured equivalent widths

(≥ 300 eV), the inclination angle of Cyg X-3 would have to be $\geq 85°$ (Vrtilek et al. 1993). The line emission is broadened by scattering in a thin corona in the outer parts of the disk.

5.3. *Iron Absorption Edges*

Two absorption edges, one due to Fe I at ≈ 7.1 keV and another due to Fe XXVI at 9.2 ± 0.1 keV, have been clearly detected in both the "high" and the "low" state. The τ_{m1}, maximum depth of absorption for the cold iron is slightly higher in the "high" state. Significant binary modulation is seen only in the "high" state. The ionized iron edge does not show significant change in the two intensity states nor does it show significant modulation, but the same trend as that of the neutral iron edge is indicated in the data. Therefore, the iron absorption—both neutral and ionized, can arise from the outer parts of the accretion disk corona having different ionization regions.

The intensity of the Kα line (I_{line}), through recombination after photoionization from helium-like iron in a uniform matter surrounding a continuum X-ray emitter, is estimated to be (Basko 1980)

$$I_{line} = (N_{Fe}/10^{19.8})(\Omega/4\pi)I_{abs}\eta ,$$

where N_{Fe} is the number of Fe atoms in the line of sight, Ω is the solid angle of Fe material subtended at the source, I_{abs} is the intensity absorbed above K-shell energy, and η is the efficiency. We calculate that the expected I_{line}/I_{abs} for Fe XXVI is 0.15 and 0.17 in the "low" and "high" states, respectively, from the observed absorption edge depths by keeping $\eta = 0.5$ and $\Omega = 4\pi$. We also estimate that the value of I_{abs} is 0.0143 and 0.0144 photons cm^{-2} s^{-1} in the "low" and "high" states, respectively (for Fe XXVI). From the line emission parameters (Table 4) we can derive I_{line}/I_{abs} of 1.28 and 1.72 for the "low" and "high" states, respectively. Therefore, we see that the I_{line}/I_{abs} observed is higher than that expected (by a factor of ~ 10). A similar discrepancy is also deduced from the *Tenma* observations, and this can be reconciled with some peculiar geometry such that matter with higher iron column density exists out of the line of sight (Kitamoto et al. 1987).

For the cold Fe, the values of I_{line}/I_{abs} estimated from the absorption edges are 0.19 and 0.21 for "low" and "high" states, respectively. Since there is no evidence for Fe I line emission in the data, we have estimated the 90% confidence level upper limits as 0.0023 and 0.0051 photons cm^{-2} s^{-1} in the "high" and "low" states, respectively. This leads to upper limits for the values of I_{line}/I_{abs} as 0.05 and 0.19 (for the two states). The ratio is lower than that expected from the edges by a factor of 3.8 for the "low" state, and it is comparable to the expected value in the "high" state. Though a peculiar geometry cannot be ruled out, a higher resolution observation which can resolve the two lines and obtain a better measure of the variation of the absorption and emission features as a function of the binary phase would clarify the picture.

5.4. *An Overview of Spectral Regions in Cygnus X-3*

A geometrical picture showing all the spectral components of Cyg X-3 that presents itself consists of (1) a central compact hot blackbody near the surface of the neutron star where the accretion disk touches it, followed by (2) an accretion disk corona in which low-energy photons are Compton upscattered to higher energies and which shine on the accretion disk producing fluorescence of iron. The whole binary system is viewed almost along an edge through different zones of ioniza-tion of the accretion disk producing absorption edges due to iron and is immersed in ionized matter that produces little low-energy X-ray absorption. The main differences between the "high" state and the "low" state are that in the "low" state the blackbody is hotter but smaller, Comptonization region is relatively more compact and more opaque, the fluo-rescing iron is less highly ionized, and the low-energy absorp-tion is nonexistent.

6. SUMMARY

The salient features of the paper can be summarized as follows.

1. We have made a thorough analysis of the X-ray spectrum of Cyg X-3, during its two intensity states ("high" and "low"), using *EXOSAT* data.

2. We have made a *joint fit* to the data from the argon, xenon detectors of ME and the GSPC after performing a reli-able mutual detector calibration of the gains and effective areas correct to 0.6% and 1%, respectively. Small variations of the gain of the GSPC within an observation were also accommo-dated in the analysis.

3. The joint fit provides a statistically acceptable generalized model for both the states of Cyg X-3. The principal features of the generalized model are as follows:

1. A blackbody emission with temprature varying from 1.47 keV in the "high" state to 2.40 keV in the "low" state.

2. An additional continuum component from a Com-ptonized region which, when extrapolated, agrees with the hard X-ray (> 20 keV) balloon data. The CompST param-eters transit from high kT_e, low τ values in the "high" state to low kT_e and high τ values in the "low" state.

3. A Gaussian line emission due to Fe XXVI in the "high" state (energy ~ 6.95 keV) and to Fe XX–Fe XXII in the "low" state (energy ~ 6.56 keV).

4. Absorption edges at 7.1 keV (due to neutral iron) and at 9.2 keV (due to Fe XXV–Fe XXVI).

5. A common neutral hydrogen column density which is as low as the Galactic absorption in the line of sight to the source in the "low" state and about 3–4 times higher in the "high" state.

6. A low-energy thermal bremsstrahlung component with $kT \sim 0.38$ keV with a flux of $\sim 9 \times 10^{-11}$ ergs cm^{-2} s^{-1} and $< 4 \times 10^{-11}$ ergs cm^{-2} s^{-1}, for the "high" and "low" states, respectively.

4. We find that the binary modulation of the X-ray emission from Cyg X-3 can be attributed, predominantly, to the varia-tions in the intensities of its continuum components. The modulation depth is maximum for the blackbody flux. There is small, but significant, phase variation in the parameters kT_{bb}, N_H and τ_{m1}.

5. The results, when interpreted in terms of an accretion disk and a Comptonized region, suggest a view along an edge of the binary system. The change of CompST parameters from "high" to "low" state may be associated with a transition from a two-temperature thick disk corona (high kT_e, low τ) to a thin disk corona (low kT_e, high τ).

REFERENCES

Basko, M. M. 1980, A&A, 87, 330
Becker, R. H., Robinson-Saba, J. L., Boldt, E. A., Holt, S. S., Pravdo, S. H., Serlemitsos, P. J., & Swank, J. H. 1978, ApJ, 224, L113
Blisset, R. J., Mason, K. O., & Culhane, J. L. 1981, MNRAS, 194, 77
Blodin, J. M., Kallman, T. R., Fryxell, B. A., & Taam, R. E. 1990, ApJ, 356, 591
Bonnet-Bidaud, J. M., & Chardin, G. 1988, Phys. Rep., 170, 325
Chlebowski, T., Harnden, F. R., Jr., & Sciortino, S. 1989, ApJ, 341, 427
Chu, K. W., & Bieging, J. H. 1973, ApJ, 179, L21
Done, C., Mulchaey, J. S., Mushotzky, R. F., & Arnaud, K. A. 1992, ApJ, 395, 275
Elsner, R. F., Ghosh, P., Darbro, W., Weisskopf, M. C., Sutherland, P. G., & Grindlay, J. E. 1980, ApJ, 239, 335
Fryxell, B. A., & Taam, R. E. 1988, ApJ, 335, 862
George, I. M., & Fabian, A. C. 1991, MNRAS, 249, 352
Harnden, F. R., Jr., et al. 1979, ApJ, 234, L51
Hermsen, W., et al. 1987, A&A, 175, 141
Kallman, T. R., & McCray, R. A. 1982, ApJS, 50, 263
Kallman, T., & White, N. E. 1989, ApJ, 341, 955
Kitamoto, S., Miyamoto, S., Matsui, W., & Inoue, H. 1987, PASJ, 39, 259
Kitamoto, S., Mizobuchi, S., Yamashita, K., & Nakamura, H. 1992, ApJ, 384, 263.
Lauque, R., Lequeux, J., & Rieu, N. Q. 1972, Nature Phys. Sci., 239, 119
Mauche, C. W., & Gorenstein, P. 1986, ApJ, 302, 371
Melia, F., Zylstra, G. J., & Fryxell, B. 1991, ApJ, 377, L101
Mitsuda, K., et al. 1984, PASJ, 36, 741
Mitsuda, K., Inoue, H., Nakamura, N., & Tanaka, Y. 1989, PASJ, 41, 97
Molnar, L. A., & Mauche, C. W. 1986, ApJ, 310, 343
Morrison, R., & McCammon, D. 1983, ApJ, 270, 119.
Peacock, A., et al. 1981, Space Sci. Rev., 30, 525
Rao, A. R., Agrawal, P. C., & Manchanda, R. K. 1991, A&A, 241, 127
Sanford, P., Mason, K. O., & Ives, J. 1975, MNRAS, 173, 9P

Serlemitsos, P. J., Boldt, E. A., Holt, S. S., Rothschild, R. E., & Saba, J. L. R. 1975, ApJ, 201, L9
Shafer, R. A., Haberl, F., Arnaud, K. A., & Tennant, A. F. 1991, ESA publication TM-09
Shakura, N. I., & Sunyaev, R. A. 1973, A&A, 24, 337
Shapiro, S. L., Lightman, A. P., & Eardley, D. M. 1976, ApJ, 204, 187
Singh, K. P. 1992, private communication
Singh, K. P., Rao, A. R., & Vahia, M. N. 1991, ApJ, 377, 417
Smith, A., & Parmar, A. N. 1985, EXOSAT Express, 10, 40
Stella, L., & Rosner, R. 1984, ApJ, 277, 312
Sunyaev, R. A., & Titarchuk, L. G. 1980, A&A, 86, 121
Taam, R. E., & Fryxell, B. A. 1988, ApJ, 327, L73
Turner, M. J. L., Smith, A., & Zimmermann, H. U. 1981, Space Sci. Rev., 30, 513
van der Klis, M., & Bonnet-Bidaud, J. M. 1989, A&A, 214, 203
van der Klis, M., & Jansen, F. A. 1985, Nature, 313, 768
van der Klis, M., Peacock, A., Smith, A., White, N., Mason, K., & Manzo, G. 1985, Space Sci. Rev., 40, 297
van Kerkwijk, M. H., et al. 1992, Nature, 355, 703
Vrtilek, S. D., Soker, N., & Raymond, J. C. 1993, ApJ, 404, 696
White, N. E. 1985, EXOSAT Express, 11, 51
White, N. E., Becker, R. H., Boldt, E. A., Holt, S. S., Serlemitsos, P. J., & Swank, J. H. 1981, ApJ, 247, 994
White, N. E., & Holt, S. S. 1982, ApJ, 257, 318
White, N. E., & Peacock, A. 1988, Mem. Soc. Astr. Italiana, 59, 7
White, N. E., Peacock, A., Hasinger, G., Mason, K. O., Manzo, G., Taylor, B. G., & Branduardi-Raymont, G. 1986, MNRAS, 218, 129
White, N. E., Peacock, A., & Taylor, B. G. 1985, ApJ, 296, 475
White, N. E., Stella, L., & Parmar, A. N. 1988, ApJ, 324, 363 (WSP)
Willingale, R., King, A. R., & Pounds, K. A. 1985, MNRAS, 215, 295